

Assessment of the Efficiency of Solar Radiation Concentrating System

by

Célia Domingas Artur

Submitted in fulfillment of the academic
requirements for the degree of
Master of Science in the
School of Physics,
University of Kwazulu – Natal
Durban

December 2009

As the candidate's supervisor I have approved this dissertation for submission

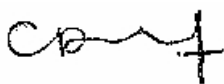
Signed: _____ Name: _____ Date: _____

Declaration

I, Célia Domingas Artur, student number: 207512359 declare that

1. The research reported in this thesis, except where otherwise indicated, is my original research.
2. This thesis has not been submitted for any degree of examination at any other university.
3. The thesis does not contain others persons' data, picture, graph or other information, unless specifically acknowledged as being sourced from other persons.
4. This thesis does not contain others persons' writing, unless specifically acknowledged as being sourced from other researchers. Where other written source has been quoted, then:
 - a. Their word have been re-written but the general information attributed to them has been referenced
 - b. Where their exact words have been used, then their writing has been placed in italics and inside quotation marks, and referenced.
5. This thesis does not contain text, graphics or tables copied and pasted from internet, unless specifically acknowledged, and the source being detailed in the thesis and in the references sections.

Signed.....



...

Dedication

This research is dedicated to the memory of my mother and to my father

Acknowledgements

A lot of people have contributed to this research project being a reality. I would like to thank my Supervisor, Professor Sadha Pillay for his patience, guidance, especially when writing up this thesis. My gratefulness is also extended to my co-supervisor, Professor Jørgen Løvseth, for his fruitful advices throughout the course of this work. Thank you very much.

I am also grateful to all staff of the Department of Physics of the University of KwaZulu-Natal (Westville Campus) especially to Mr. E. Zhandire for his advices and fruitful discussions. I am also grateful to Mr. Danny Padaya Chee from central academic workshop of the University of KwaZulu-Natal (Westville Campus) for technical support during the installation of the system.

I want to acknowledge the University of Eduardo Mondlane in Mozambique through the Renewable Energy program for financial support. I also thank my colleagues Mr. J. Doho, Ms. S. Bila and Mr. M. Macome for assistance in drafting up this thesis. I am also grateful to Dr. B. Cuamba for his assistance.

Finally, special thanks go to my family for all love and support. To my dear “fiancé” J. Chivale, thanks for being there when I needed you.

Abstract

A Solar Radiation Concentrating System for generation of high temperature heat for a solar oven was developed and evaluated at the University of KwaZulu-Natal, Westville Campus, Durban - South Africa. The system concentrates direct solar radiation on a small area receiver which absorbs the radiation and converts it into thermal energy that may be stored and used for several applications where food preparation and water pasteurization is the priority.

The concentrator, area 2.2 m^2 , is a half satellite communication dish covered with trapezoidal acrylic mirror tiles. The receiver/absorber is a spiral coil of blackened stainless steel pipe. Oil is circulated as heat transfer fluid.

To determine the optimal dimension and position of the receiver, two experimental methods were used:

- (1) The tiles were scanned using a vertical, self adjusting laser beam to get a distribution of reflected radiation across the focal volume.
- (2) A thin, blackened stainless steel plate was placed at appropriate distances in the focal volume, and temperature distribution scanned using a temperature gun.

The latter method proved to be the more useful.

Results of the analysis of system performance showed that the system has the capability to produce high temperatures for domestic purposes. The efficiency of the system is about 35 %.

Chapter 1	1
Introduction.....	1
1.1 Design of solar thermal systems and solar thermal electricity delivered.....	2
1.1.1 Small scale concentrating systems.....	2
1.1.2 Large scale concentrating systems.....	3
i) Parabolic trough.....	3
ii) Central receivers.....	4
iii) Parabolic dish.....	5
1.2 Motivation and justification: Energy in Mozambique as example	6
1.3 Aims and objectives	7
1.4 Brief description of the constructed solar concentrating system	7
1.5 Thesis outline	8
Chapter 2	9
Solar Energy	9
2.1 The sun.....	9
2.2 The extraterrestrial solar radiation	10
2.3 The solar radiation at the surface of earth.....	11
2.3.1 Attenuation by atmosphere	11
a) Components of solar radiation.....	12
2.3.2 Spatial and temporal distribution	13
2.4 Availability of solar Energy in Mozambique.....	15
2.5 The solar radiation collection.....	16
Chapter 3	20
Solar Concentrating Collectors	20
3.1 General introduction	20
3.1.1 Reflection of energy to the receiver.....	21
a) Limit of Concentration ratio	21
3.2 Parabolic dish concentrating collector	22
3.2.1 The concentrator geometry	22
3.2.2 Reflection of energy to the receiver: Focal flux distribution.....	25
3.2.3 Tracking mechanism.....	25

Chapter 4.....	27
Description and Construction of the System	27
4.1 General.....	27
4.1.1 The concentrator design and construction	28
a) Design	28
b) Construction.....	30
4.1.2 The receiver	30
a) Determination of focal length and receiver dimensions	31
b) Receiver design and construction	37
4.1.3 The thermal storage.....	39
4.1.4 The receiver and the heat transfer fluid circuit	41
4.1.5 Pumping process	46
4.1.6 Tracking mechanism.....	48
4.2 Installation of the half-dish collector	48
4.2.1 Environmental stability	48
4.3 Data acquisition	49
4.3.1 Temperature measurement.....	52
4.3.2 Flow rate measurement	52
4.3.3 Direct solar radiation measurement	57
4.4 Efficiency of the solar radiation concentrating system.....	58
Chapter 5.....	60
Results and Discussion	60
5.1 Efficiency of the system.....	73
Chapter 6.....	75
Conclusions and Future Work	75
References.....	77

Chapter 1

Introduction

One of the greatest challenges of the world today is energy supply. The fossil fuels, which are currently the main source of energy, besides causing negative impacts on the environment, has been rising in price during last years [BBC News]. On the other hand, the biomass energy which is the main source of energy in developing countries; is becoming scarce. Solar energy, in particular solar thermal energy, is one of the primary alternatives to biomass. It is environmentally clean, affordable and sustainable.

A considerable amount of solar thermal energy can be produced according to needs using solar collectors such as flat-plates or solar concentrating collectors. Flat-plate systems are practical for applications requiring moderate temperatures, in the 50 to 100°C range [Imadojemu, 1995]. Frequently, temperatures above this range are necessary in applications. In this case, solar concentrating systems are a better choice, since temperatures above 700°C [Twidell and Weir, 2006] can be achieved.

Solar concentrating systems typically comprise a concentrator, which is an optical system made of reflective (or refractive) material, a receiver and sometimes a thermal storage. The incident radiation falling onto the concentrator is reflected to the receiver. The receiver absorbs the radiation and converts it into thermal energy. The thermal energy can be stored using a thermal storage. Appropriate tracking systems are used to orientate the collector to follow the sun.

This system can be very useful for rural families, mainly in developing countries situated in Sunbelt (between latitudes 40° north to 40° south) [Cuamba et al, 2006], where the

electricity grid is costly and unfeasible. In those areas, the thermal energy can be used for several applications, primarily for food preparation and water pasteurization.

1.1 Design of solar thermal systems and solar thermal electricity for heat and electricity production

1.1.1 Small scale concentrating systems

Small scale solar thermal energy systems (solar cookers) are being widely used in some countries such as India, China and Spain. The effective energy output of this type of systems, is appropriate for rural areas where the demand for energy is lower, due to low population density. The first solar kitchen using reflective materials was designed and produced in the 1950s and improved in the 1960s and 1970s, but has limitations due to its complexity [Arenas, 2007]. Years later, many designs were tested like box and parabolic types. The design, development and testing of a portable parabolic solar kitchen is detailed by Arenas [2007]. The prototype reaches the average energy of 175 W and the efficiency of 26.6%.

In Africa, one of the successful solar cookers that have been used mainly for refugees in Kenya, Namibia, Malawi, Chad, and Sudan is the Cookit [Toonen, 2009]. The Cookit was designed in 1994, by Roger Bernard in cooperation with Solar Cookers International. Cookit is a box- type cooker covered with aluminum foil which reaches temperatures from 70°C to 90°C [Toonen, 2009].

Franco et al [2008] reported a low cost parabolic concentrator for pasteurization of goat milk using a consecutive aluminum cones. The concentrator cooks large portions of food using a vaporizer located at focus.

The enormous advantages of solar cookers includes: it is a pollution-free alternative (smoke free cooking, decreasing of deforestation); solar radiation is free; saving of time since food can be left cooking and will never burn; stirring of food is not required and

conservancy of nutritional value of food. Despite the mentioned advantages of solar cookers the acceptance of this technology is still limited. This is largely due to the intermittent nature of sunshine; food cannot be prepared late evening or during cloud days. To solve these temporal problems, concentrating systems that stores energy are needed in way to give reliability to the solar cookers. Unfortunately solar cookers with energy storage systems are still in experimental and developmental stage [Kulkarni et al, 2008].

Ramadan et al [1988] developed a solar cooker with a medium heat storage using local materials in Tanta University. The cooker achieved approximately 3 hours cooking indoor with efficiency up to 28.4%. Buddhi and Sahoo [1997] designed a solar cooker with latent heat storage, appropriate for the climatic conditions in India. Several other designs have been proposed by [Bushnell, 1992, Domanski et al., 1995 and Scheffler, 2006].

1.1.2 Large scale concentrating systems

The first large concentrators were installed in the 1980s [Mills, 2004]. From then till now few has been made commercially due to market resistance and poor political and financial support programs [Mills, 2004], but scientifically several prototypes have been developed and tested. Three designs of concentrators are most used: parabolic troughs, central receivers and parabolic dishes.

i) Parabolic trough

Parabolic trough has a parabolic cross section (U-shaped) to concentrate the solar radiation in line focus. Usually the concentrator is made up of coated silver or polished aluminum. The orientation is done using one axis tracking system. The receiver is a metal absorber surrounded by a glass tube with axis in the focal line. The axis is parallel to the concentrator aperture. This design is comparatively easier to construct for large systems, since the reflector is only curved in one direction. It is also most common commercially available [Mills, 2004].

The most mature and successful solar thermal electricity technology is the LS-3 plant (Figure 1.1) installed in 1984, in California by LUZ International, Inc. with 354 MWe of capacity. It is believed that the future cost in large production will be US\$0.055/kWh in areas of high insolation as result of large scale production and design improvements [Mills, 2004].

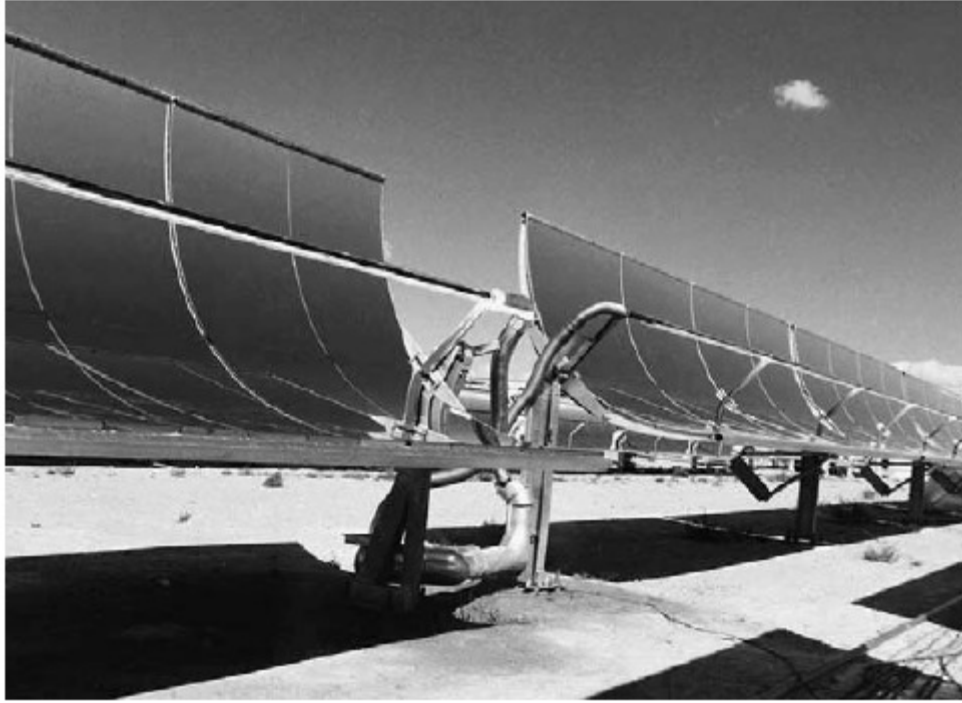


Figure 1.1: A portion of an LS-3 plant at Kramer Junction, California (source: Mills 2004)

ii) Central receivers

Central receivers also called power tower technology consist of hundreds or thousands of large tracking mirrors, known as heliostats. The heliostats reflect the beam radiation to a single focal zone. The focal zone is mounted over the heliostats field to avoid interference between the reflected rays.

The first most successful power tower was Solar One (11.7 MW_e) placed at Barstow in California (Figure 1.2). Solar One was converted in Solar Two in the 1990_s, using molten

salt storage, allowing delivering of electricity during the evening or in clouded periods [Mills, 2004].



Figure 1.2: The Solar Two central receiver plant in Barstow, California (source: Mills 2004).

iii) Parabolic dish

Parabolic dish concentrating collector is a three-dimensional system, which uses a reflector surface with paraboloid of revolution shape to concentrate solar radiation to a supposed focal point where the receiver is placed. The dish concentrator aperture is always orientated perpendicularly to the direct solar radiation by using a two axis tracking system. This system is advantageous over other systems, largely due to its focal point system and the absence of cosine losses. The biggest challenge in the construction of the parabolic dish concentrator is to achieve a good parabolic shape, since the surface curvature varies in different regions of the paraboloidal shape. For small systems, paraboloidal backing is easily produced by a press shaping. In practice, it is easier to

construct a dish reflecting surface by using small elementary mirrors (tiles) compared to using a single continuous mirror.

Potentially, parabolic dish is one of the solar thermal technology options that can provide high temperatures in range of 340 to 1200 K [Norton, 2001]. One successful dish concentrator has been the Australian National University (ANU) paraboloidal dish technology (Figure 1.3) [Mills, 2004].

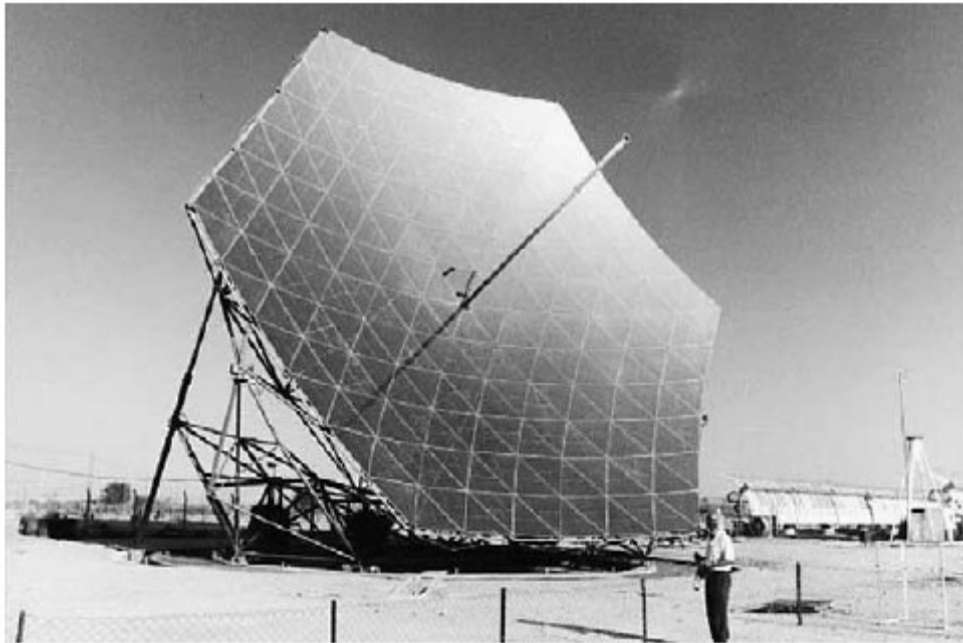


Figure 1.3: The ANU SG3 dish installed at Sede Boqer in Israel (source: Mills 2004).

1.2 Motivation and justification: Energy in Mozambique as example

The demand of energy resources that are affordable, efficient and environmentally clean is the principal focus today. Mozambique has enormous energy resources. The hydroelectric of Cahora Bassa is one of the largest installations in Africa, with 2,075MW. In addition, Mozambique has reserves of natural gas and coal that are being exploited. Even with this Mozambique's huge production of electricity, 80% [National Directory of Energy, 2006] of the Mozambican population lives in rural areas where the electricity

from conventional grid is not available and the oil or coal products are not affordable. In general, the conventional power grid provides about 12% of the energy needs. All other needs are covered by traditional fuels (wood and charcoal). These traditional sources of energy have a number of harmful effects on the people's health and environment (as deforestation and air pollution). Furthermore, forests will no longer withstand the uncontrolled exploitation to respond to the high demand. Some areas have lack of wood for fuel due to the climatic conditions.

1.3 Aims and objectives

The aim of this study is to construct and evaluate the efficiency of a low cost small scale solar concentrating system for rural communities in developing countries where the electricity is not viable. The evaluation of the efficiency of the system concerns essentially on measuring the useful energy gain and the heat losses of the system.

The specific objectives of the research work are:

1. to design and construct the concentrator;
2. to determinate the concentrator focal length;
3. to determine the receiver dimensions;
4. to design and construct the receiver;
5. to evaluate the efficiency of the system.

The storage was already developed and tested.

1.4 Brief description of the constructed solar concentrating system

Among the three designs of solar systems discussed before, parabolic dish is more appropriate for rural communities due to its temperature range. A small scale concentrating system can deliver 4 to 50 kW, which is enough to cover many needs in rural areas of developing countries [Cuamba et al, 2008]. The solar concentrating system in this study was started from an earlier design by Robert van den Heetkamp. van den

Heetkamp designed and mounted the entire structure carrying the concentrating collector (Figure 4.15). The concentrator is a half parabolic dish with an aperture diameter of 2400 mm. In this project the concentrator is covered by trapezoidal tiles of acrylic mirror material. The receiver (absorber) is a stainless steel spiral coil of diameter 250 mm, which heats up the oil circulating. The oil is Calflo Heat Transfer Fluid. The maximum operating temperature of the oil is about 326° C [website 2]. The storage is pre-existent rock bed thermal storage detailed at Mawire [2005]. The storage had been constructed and tested with a hot plate simulating a solar concentrating collector. In the current work, the hot plate was replaced by a parabolic dish concentrating collector (half dish).

1.5 Thesis outline

The thesis consists of 6 chapters. The introduction motivates the need for this study. Chapter 2 provides theoretical concepts about the solar energy resource and its availability at the earth's surface. Chapter 3 discusses solar concentrating collectors, especially parabolic dish concentrating collectors which is the central topic of this research.

Chapter 4 is a description of the system constructed and all experimental methods and procedures carried out. Two experimental methods to determine the concentrator focal length and the receiver dimensions are detailed. Parameters measured in the evaluation of the dish concentrator and the data acquisition instrumentation are also discussed in this chapter.

Chapter 5 presents discussion of the results. This chapter also analyzes and evaluates the efficiency of solar radiation concentrating system. To finalize, chapter 6 gives the conclusions and recommendations for further work.

Chapter 2

Solar Energy

This chapter presents the availability of solar energy resource at the earth's surface. The first section reports the origin of solar energy resource, while the section 2.2 gives the amount of solar energy on top of earth atmosphere. This amount is attenuated by several factors, thus, section 2.3 is on the amount of solar radiation that reaches the earth surface. Section 2.4 gives the availability of solar energy in Mozambique as an example. The last section focuses on collection of solar energy on any surface.

2.1 The sun

The sun is placed at the core of the solar system with a diameter of 1.39×10^9 m [Duffie and Beckman, 1991]. It is composed of different gases: hydrogen (73.46%), helium (24.85%), oxygen (0.77%), carbon (0.29%), iron (0.16%), neon (0.12%) and nitrogen, silicon, magnesium, sulfur, etc ($< 0.1\%$) [Stine and Geyer, 2001]. The temperature in the interior of the sun is estimated to be in range of 8×10^6 to 40×10^6 K [Duffie and Beckman, 1991] and the density is about 1600 Kg/m^3 [Stine and Geyer, 2001].

The solar radiation is the result from several and continuous fusion reactions of the gases. Hydrogen fusion is the most important reaction process which forms helium. In this process, the mass of the resulted helium is less than the mass of hydrogen. The hydrogen “mass loss” in the reaction (in rate of about 4.1×10^9 kg/s) [Stine and Geyer, 2001] is converted to heat. The end result of this process is described by equation (2.1) [Stine and Geyer, 2001] as:



2.2 The extraterrestrial solar radiation

The sun and the earth are surrounded by layers of gases known as sun and earth atmosphere respectively. Solar radiation incident outside the earth's atmosphere is called extraterrestrial solar radiation.

The high temperature heat in the interior of the sun is transported to the surface and is radiated. The surface temperature of the sun is about 5800K [Twidell and Weir, 2006] and is a source of radiation with a relatively continuous spectral distribution.

In the electromagnetic spectrum the energy rich part of the solar radiation spectrum comprises wavelengths between 0.3 to 3 μm . These wavelengths are divided into three main regions: the ultraviolet region ($< 0.38 \mu\text{m}$), the visible region ($0.38 \mu\text{m}$ to $0.78 \mu\text{m}$) and the infrared region ($> 0.78 \mu\text{m}$) [Duffie and Beckman, 1991]. Figure 2.1 shows the spectral distribution of the extraterrestrial solar radiation. The area under the curve corresponds to the value of solar constant, estimated at 1367 W m^{-2} [Duffie and Beckman, 1991].

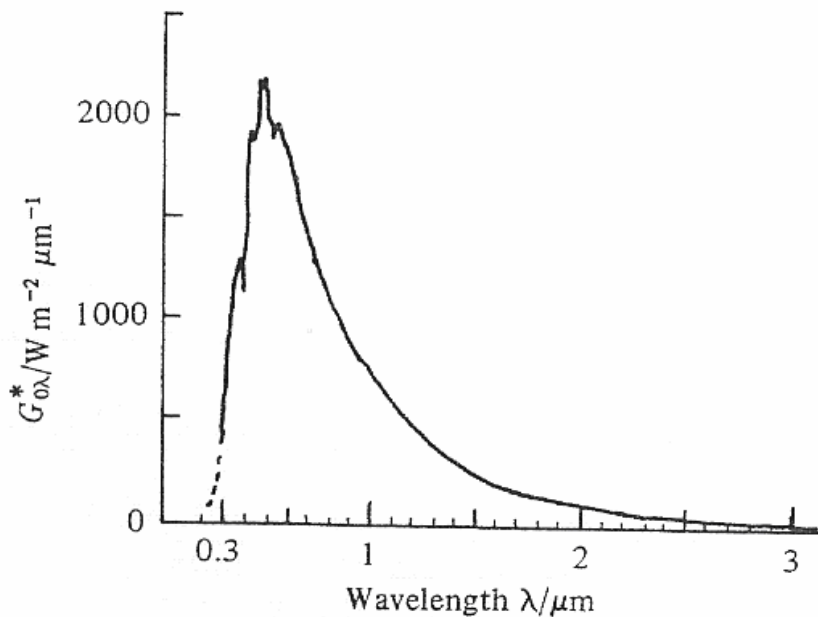


Figure 2.1: Spectral distribution of extraterrestrial solar irradiance (source: Twidell and Weir 2006)

The solar constant is defined as the energy incident from the sun on unit area of surface perpendicular to the direction of propagation of the radiation, per unit time, at mean sun-earth distance (1.495×10^{11} m), outside of the atmosphere [Duffie and Beckman, 1991].

2.3 The solar radiation at the surface of earth

Part of radiation from the sun that reaches the earth's surface depends on several factors, such as the state and composition of the atmosphere, geographic location, time of day, etc. The wavelength range of the solar radiation spectrum at the earth surface important for energy purposes is 0.29 to 2.5 μm [Duffie and Beckman, 1991].

2.3.1 Attenuation by atmosphere

Solar radiation in the atmosphere is modified due to three main processes: absorption, reflection, and scattering.

Absorption is the process by which the radiation is retained and converted to heat by a substance. A significant amount of solar radiation is absorbed by ozone in the ultraviolet band and by water vapor and carbon dioxide in infrared [Duffie and Beckman, 1991] reducing the amount of solar radiation that reaches the earth surface.

Scattering occurs when small particles and gas molecules diffuse part of the incident solar radiation. A significant fraction of scattered solar radiation is returned back to space. The end process is called reflection. Most of the reflection occurs when the radiation is intercepted by clouds. Globally, 30% is reflected, 20% absorbed in atmosphere and 50% absorbed in earth surface [Macdonald and Sertorio, 1990].

The level of occurrence of these processes depends on the number of the atmospheric components through which radiation must cross (referred as temporal conditions of the atmosphere), its dimension in relation to wavelength of radiation [Duffie and Beckman, 1991] and the altitude of the observer above sea level.

a) Components of solar radiation

In general, the solar radiation has two components, a beam solar radiation (also called direct solar radiation) that comes directly from the sun disc and a diffuse solar radiation (or scattered) that come out from all directions of the sky.

The beam solar radiation is the radiation received directly from the sun without having been dispersed by the atmosphere. This component is important in the design of the solar energy systems that operate at high temperatures, because it can be focused and concentrated in small areas, using reflective materials. The diffuse radiation is received from the sun after its direction has been changed by atmosphere.

On clear, dry days the direct solar radiation at midday is reduced by 30% by the atmosphere and during thick, cloudy days, almost completely. Figure 2.2 gives an example of the two components of solar radiation in a clear day. The solar radiation data were obtained from the radiometric station at Eduardo Mondlane University, Physics Department, Maputo - Mozambique on 14th April 2006. The maximum value of direct solar radiation (orange color curve) is about 900 W/m^2 and the diffuse radiation (pink color curve) is about 10% of the direct solar radiation value.

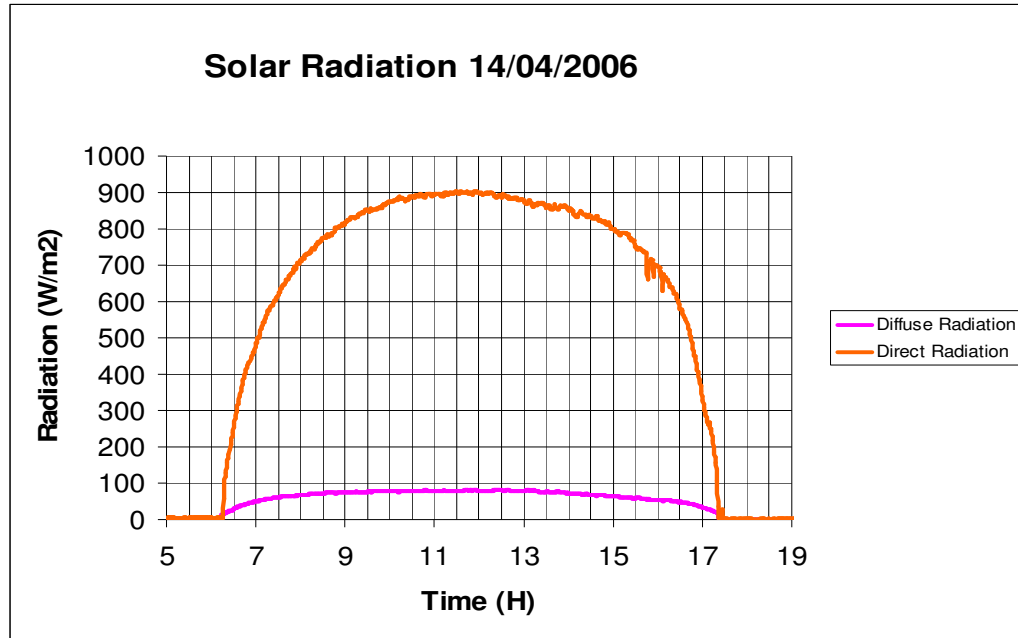


Figure 2.2: Temporal distribution of direct and diffuse solar radiation in a clear day (Solar Radiation data obtained from the radiometric station at Eduardo Mondlane University, Physics Department, Maputo-Mozambique; 14th April 2006)

2.3.2 Spatial and temporal distribution

The surface solar radiation is not uniformly distributed geographically. The amount of solar radiation in a given locality is a useful input to evaluate and exploit the solar energy potential. To characterize the surface radiation intensity, the earth is divided into four sets of belts with respect to latitudes. The first, with best conditions of sunshine is the belt between 15° and 35° latitudes south and north of the equator. The second set with a belt with good conditions of sunshine covers latitudes between 15° south and 15° north of the equator. In this belt the proportion of scattered radiation is quite high because the humidity is high, and cloud cover is frequent. The third set lies between 35° and 45° both sides of equator. The belts with least intensity of solar radiation compared to the others are located more than 45° south and north of equator [website 3].

In the temporal distribution, the maximum value possible of solar radiation incident per unit area on a surface is achieved at solar noon and the minimum at night when the sun is below horizon. These temporal variations of solar radiation intensity can be described in

terms of atmospheric air mass, which is the ratio of the distance that solar radiation passes through the earth's atmosphere to the distance it would pass if the sun were directly overhead. The radiation coming from directly overhead passes through 1 air mass at sea level and the radiation from horizon passes a major amount of air mass, more than 30 air masses [Stine and Geyer, 2001]. Therefore, the solar radiation intensity increases with the angle between the horizontal plane and the line to the sun, the solar altitude angle. For height angle, 0 to 80° the solar mass is to a good approximation to $1/\cos$ (height angle). Figure 2.3 gives the temporal distribution of the solar radiation in a clear sky day. The Solar Radiation data were obtained from the radiometric station at Eduardo Mondlane University, Physics Department, Maputo- Mozambique on 14th April 2006. In this Figure it is clearly seen that the maximum value of solar radiation intensity is achieved at solar noon (almost 12:00 hours) and the minimum at sunrise and sunset (almost 7 and 17 respectively).

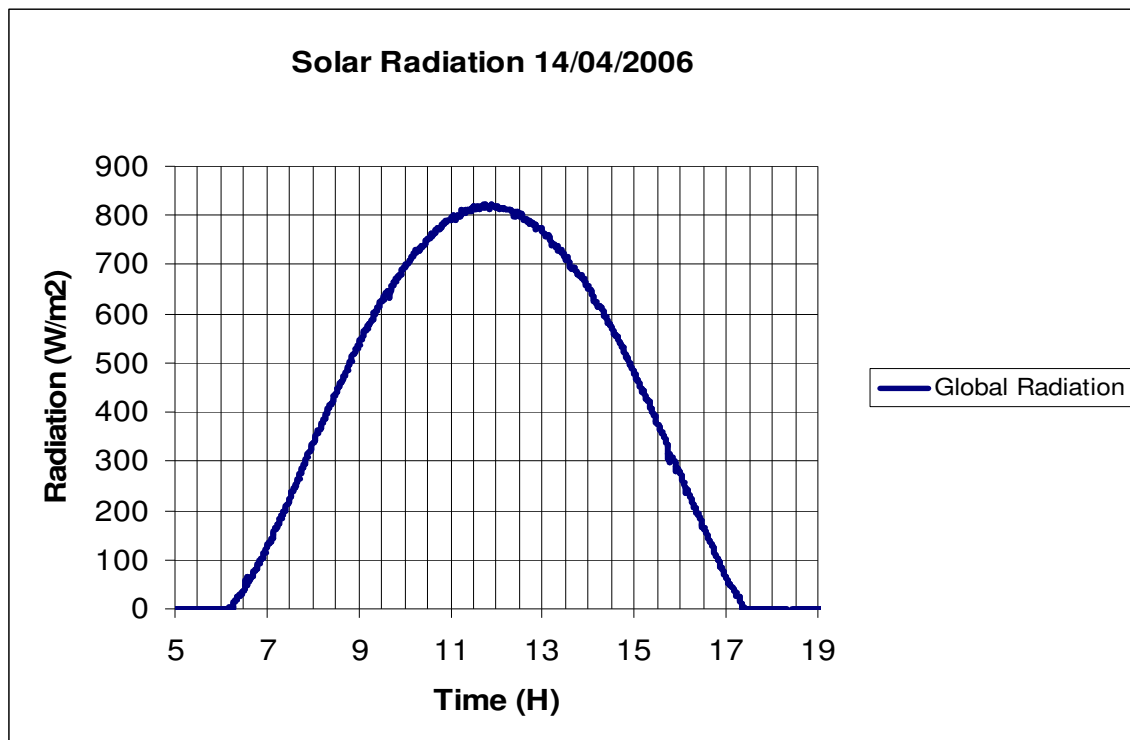


Figure 2.3: Temporal distribution of global solar radiation in a clear day (Solar Radiation data obtained from the radiometric station at Eduardo Mondlane University, Physics Department, Maputo- Mozambique; 14th April 2006)

2.4 Availability of solar energy in Mozambique

Mozambique is geographically located inside the Sunbelt of best and good conditions of sunshine on the earth surface, between the latitudes $10^{\circ}12'$ and $26^{\circ}52'$. These Sunbelts are located in tropical and equatorial regions. The tropical region is climatically in semi-arid regions where cloud coverage and precipitation are scarce. More than 90% of solar radiation is direct solar radiation. The hours of sunshine per year are over 3000 [Website 3]. The equatorial regions have higher scattering of solar radiation due to high humidity and predominance of clouds. There is about 2500 hours of sunshine per year [Website 3]. Mozambique may be considered to have favorable conditions of sunshine. The average of sunshine is 7 to 9 hours per day [Nijegorodov et al, 2003]. Figure 2.4 shows the simulated results for 21 synoptic stations in Mozambique. The stations are presented in the form of maps of monthly mean daily direct beam radiation for December and June [Nijegorodov et al, 2003].

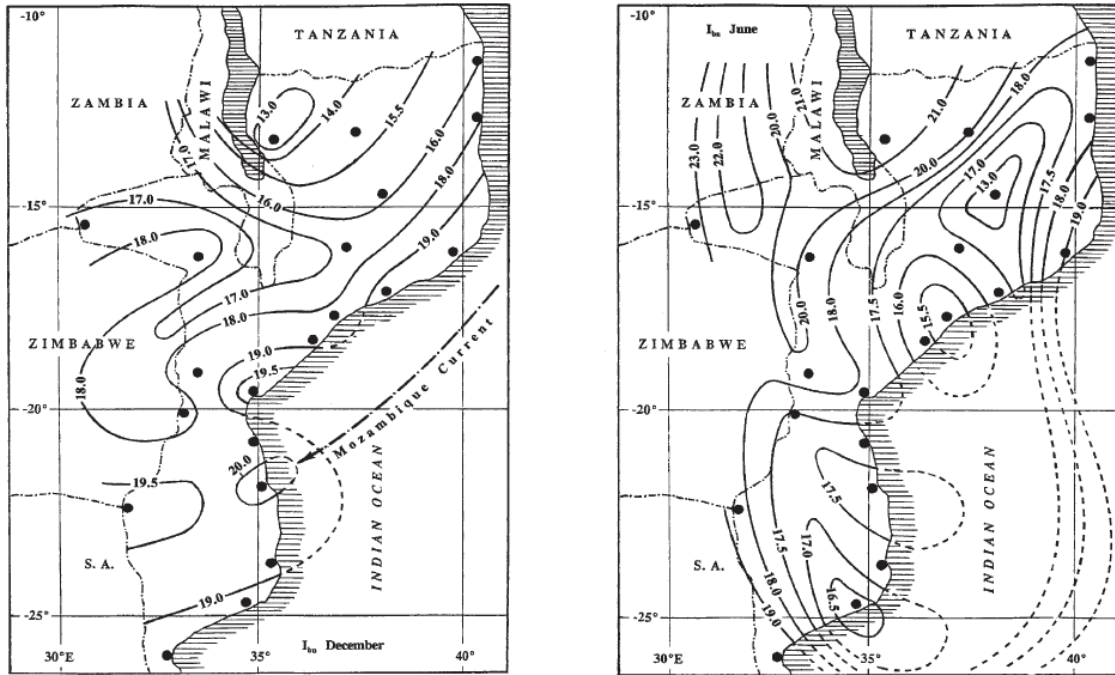


Figure 2.4: Maps of monthly mean daily direct beam normal radiation for December (left) and June (right) for Mozambique. Values indicated are in MJ m^{-2} [source: Nijegorodov et al, 2003].

2.5 The solar radiation collection

To collect solar energy it is necessary to understand the location of the sun in relation to the collector. The position of the sun relative to a plane of any particular orientation to the earth can be described by several angles namely, the latitude (ϕ), the hour angle (ω), the solar altitude angle (α_s), the zenith angle (θ_z), the solar azimuth angle (γ_s), the surface azimuth angle (γ), the slope angle (β) and the angle of incidence (θ) as shown in figure 2.5.

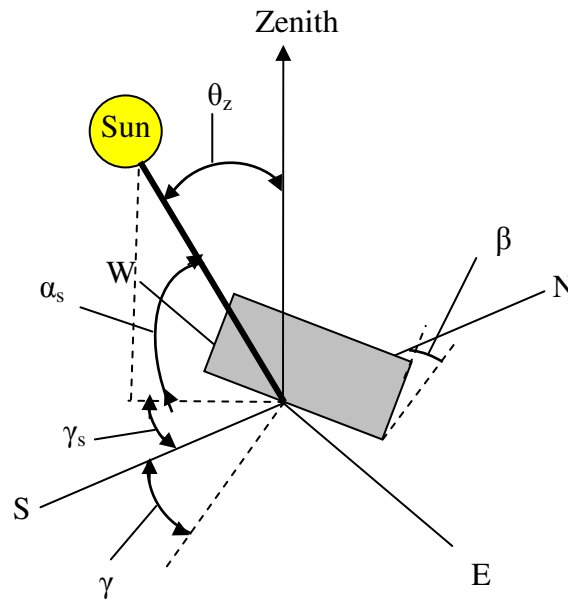


Figure 2.5: Zenith angle, solar altitude angle, slope, surface azimuth angle, and solar azimuth angle for a tilted surface.

The hour angle (ω) can be defined as the angular dislocation of the sun east or west of the local meridian. This angular dislocation is due to rotation of the earth on its axis at 1° per four minutes (15° per hour). The zenith angle (θ_z), is the angle between the vertical plane and the angle to the sun. The zenith angle varies from 0° , when the line to the sun is perpendicular to the horizontal surface, to 90° when the sun is in horizon [Duffie and Beckman, 1991].

The solar azimuth angle (γ_s) is the angular distance from south of the projection of beam radiation on the horizontal plane, while the surface azimuth angle (γ) is the deviation of the projection on horizontal plane of the normal to the surface from the local meridian, measured from the south. Conventionally the surface azimuth angle is negative for surfaces facing east and positive for west, varying from -180° to 180° [Duffie and Beckman, 1991]. The surface azimuth angle for a day depends on the latitude, declination, and the solar azimuth angle.

The slope (β) is the angle between the plane of the surface in question and the horizontal. The slope varies from 0° to 180° , with value less than 90° when the surface has an upward facing a component and greater than 90° otherwise. In the collection of energy, the angle of incidence is very important, since gives the angle between the rays that comes directly from the sun on a surface and the normal to that surface. Equations (2.2) and (2.3) give the relation between the angle of incidence to other angles [Duffie and Beckman, 1991] as

$$\begin{aligned} \cos \theta = & \sin \delta \sin \phi \cos \beta - \sin \delta \cos \phi \sin \beta \cos \gamma + \cos \delta \cos \phi \cos \beta \cos \omega \\ & + \cos \delta \sin \phi \sin \beta \cos \gamma \cos \omega + \cos \delta \sin \beta \sin \gamma \sin \omega \end{aligned} \quad (2.2)$$

and

$$\cos \theta = \cos \theta_z \cos \beta + \sin \theta_z \sin \beta \cos(\gamma_s - \gamma) \quad (2.3)$$

where,

$$\delta = 23.45 \sin \left(360 \frac{284 + N}{365} \right) \quad (2.4)$$

being N the number of day, $N = 1$ on 1st January and $N = 365$ on 31st December (In a leap year $N = 366$ on 31st December). For example on 1st January $\delta = -23.01$ and on second January $\delta = -22.93$.

And

$$\omega = \frac{15^\circ (t_s - 12)}{\text{seconds}} \quad (2.5)$$

being t_s the solar time in hours. From equation (2.5) it can be easily concluded that the hour angle at solar noon is zero, increasing by 15° every hour.

The conversion of the clock time (local standard time) to solar time is given by equation (2.6) as [Stine and Geyer, 2001]

$$LCT = t_s - \frac{EOT}{60} + LC + D \quad (2.6)$$

where EOT is the equation of time in minutes, LC is a longitude correction and D is equal to 1 hour if the location is in a region where daylight savings time are currently in effect, or zero otherwise [Stine and Geyer, 2001]. The equation of time (EOT) and the equation of longitude correction (LC) can be written as [Stine and Geyer, 2001]

$$EOT = 0.258 \cos \chi - 7.416 \sin \chi - 3.648 \cos 2\chi - 9.228 \sin 2\chi \quad (2.7)$$

being:

$$\chi = \frac{360^\circ (N - 1)}{365.242} \quad (2.8)$$

and

$$LC = \frac{(LL) - (LS)}{15} \quad (2.9)$$

where LL is the local longitude and LS the longitude of standard time zone meridian.

Example: In the particular case of Mozambique (Maputo), where the local longitude is about $32^{\circ}35'$ east meridian, the solar time that corresponded to 12-hour (midday) standard time on 1st January 2009 was 12:07:08 AM. The correction of standard time is + 07:08 minutes. The difference between the standard time and solar time (*EOT*) is -10:50 minutes.

Other important hour angles are at sunrise and sunset. These angles are a function of solar latitude angle and the declination angle. The sunset angle (ω_s) can be found by equation (2.10) as the angular displacement of the sun with respect to solar noon. Thus [Duffie and Beckman, 1991],

$$\cos \omega_s = -\tan \phi \tan \delta \quad (2.10)$$

Since the sunset angle is equal to the length of day from solar noon, the length of day (N) is multiplied by two, thus

$$N = \frac{2}{15} \cos^{-1}(-\tan \phi \tan \delta) \quad (2.11)$$

Chapter 3

Solar Concentrating Collectors

This chapter presents the theoretical concepts about solar concentrating collectors. Section 3.1 gives a general idea about solar concentrating collectors. Section 3.2 gives a general overview of parabolic dish concentrating collector.

3.1 General introduction

Solar concentrating collectors are heat exchange systems that transform solar radiation energy into thermal energy. These systems integrate the reflector surface (concentrator) and the receiver. The reflector surface directs the beam solar radiation onto the receiver. The receiver absorbs the solar radiation and transforms it into thermal energy. The thermal energy can be used directly or converted into other forms.

A necessary condition on the concentrator for optimal performance is that it must have high optical reflectance or refractance. To achieve this, the most suitable materials are mirrors or lenses. The simplicity and relatively low cost of mirrors make them a better choice. The receivers are usually made of selective absorbers, since the main aim is to get a high value of absorptivity and as low emissivity as possible. For that the absorptance is often increased by using specific surfaces, such as antireflecting layers, surface roughness, black bodies and porous surfaces. Some of these materials are: black chrome, black cobalt, black nickel, black copper, anodized aluminum and blue stainless steel [Morrison, 2001].

Concentrators are made large to concentrate a large amount of solar rays and the receivers are made as small as possible to achieve high temperatures and reduce heat

losses. This design is also helpful economically, since in general, the absorbing (receiver) surfaces are relatively more expensive than the reflecting surfaces (concentrator).

In order to achieve high temperatures, solar concentrating collectors must be oriented to follow the sun. The orientation can be done manually or automatically. Manual orientated systems are not accurate if compared to automated orientated systems, because manual systems must be oriented manually to follow the sun one degree every four minutes. This orientation depends to the operators.

3.1.1 Reflection of energy to the receiver

The level of concentration and consequently the temperature to be achieved depends on the concentrator shape. The most common imaging concentrators are designed in paraboloidal shape (parabolic dish concentrator) and cylindrical shape with parabolic cross section (parabolic trough concentrator).

In these concentrators, all optical rays of solar radiation parallel to its axis are reflected to the focus. This type of reflection allows them to have high optical concentration to achieve high temperatures. As result they accept direct solar radiation almost exclusively.

a) Limit of concentration ratio

The geometric concentration ratio as given by equation (3.1) is the ratio of the area of the concentrator aperture (A_a) to the area of the receiver (A_r).

$$C = \frac{A_a}{A_r} \quad (3.1)$$

The limit to the concentration ratio for oriented systems is a function of the size of the angle from which the radiation is collected (acceptance angle). From the sun an incident beam of solar radiation is a cone with an angular aperture of 0.53° . Thus, the acceptance half angle will be $\theta_s = 0.267^\circ$ [Campbell and Green, 1987]. The limit to the concentration

ratio, also called *sine law of concentration* for linear concentrators, (two dimensional) is given by:

$$C_{\max} = \frac{n}{\sin \theta_s} \quad (3.2)$$

where n is the index of refraction when the material (target) is immersed. For point focus concentrators (three-dimensional) the sine law of concentration leads to

$$C_{\max} = \frac{n^2}{\sin^2 \theta_s} \quad (3.3)$$

The equations 3.2 and 3.3 are only valid for symmetrical ideal concentrators that accept radiation within an angular cone [Nordlander, 2005].

Usually concentrators are placed in air, where $n=1$. Thus, for two-dimensional concentrators $C_{\max} \approx 216$ [Winston, 2001] and for three-dimensional $C_{\max} \approx 45000$ [Duffie and Beckman, 1991].

In practice the concentration ratio is far away from these values. This is due to non-ideal concentrator geometry. Sometimes a larger acceptance angle is needed to capture more amount of solar radiation and to better accommodate tracking and slope errors in shape of the reflector [Mills, 2001]. Thus, the concentration ratio for linear concentrators is in range of 10 to 50 and for circular concentrators varies from 50 to 1000 [Norton, 2001].

3.2 Parabolic dish concentrating collector

3.2.1 The concentrator geometry

As is known from mathematics, the surface formed by rotating a parabola around its axis is called a paraboloid of revolution. Solar concentrators having a reflective surface in

paraboloidal shape are called parabolic dish concentrators. The equation of paraboloid in x, y, z coordinates system, with z as axis of symmetry, can be expressed by:

$$z = \frac{x^2 + y^2}{4f} \quad (3.4)$$

where f is the focal distance with coordinates $(0, 0, f)$. The focal distance is defined as the distance from the focal point F to its vertex V (see Figure 3.1).

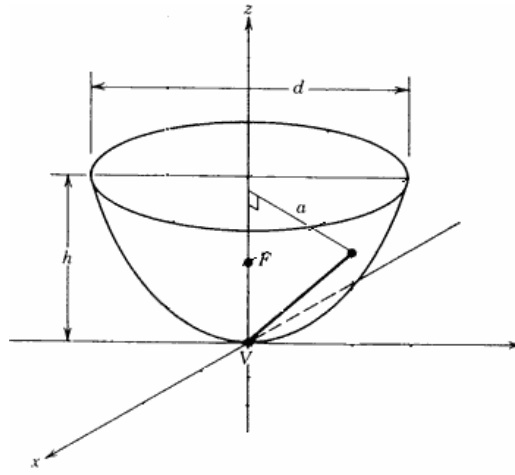


Figure 3.1: Paraboloid of revolution.

In cylindrical coordinates, where a is the distance from the z -axis illustrated in Figure 3.1, this becomes

$$z = \frac{a^2}{4f} \quad (3.5)$$

The full paraboloid surface area is calculated by equation (3.6), found by integrating equation (3.5) over appropriate limits as

$$A_s = \frac{8\pi f^2}{3} \left\{ \left[\left(\frac{d}{2f} \right)^2 + 1 \right]^{1.5} - 1 \right\} \quad (3.6)$$

where d is the aperture diameter defined in Figure 3.1. The area of the paraboloid aperture is simply the circular area defined by equation (3.7) as

$$A_a = \frac{\pi d^2}{4} \quad (3.7)$$

Parabolic concentrators are usually a truncated section of parabolic curve. The level of truncation is defined by rim angle ϕ_r , which is the angle formed by the z-axis of parabola and the P_{rim} (Figure 3.2). The level of truncation can also be expressed in terms of f/d , the ratio between the focal length and the aperture diameter (Figure 3.2). Obviously, the parabola with small rim angle will have longer focal length than its aperture diameter, and will be comparatively flat.

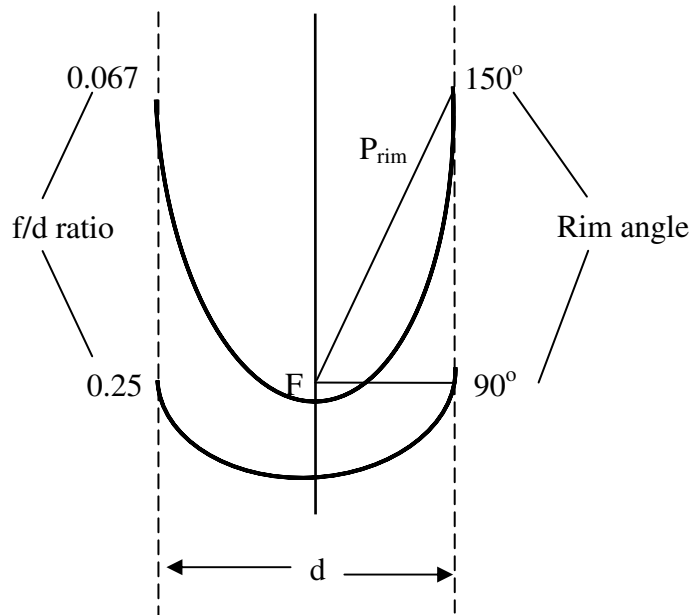


Figure 3.2: Segments of a parabola having a common focus F and the same aperture diameter (source: Stine and Geyer 2001 modified).

The rim angle may be found, considering the parabola dimensions, by the following expression:

$$\tan \phi_r = \frac{1}{(d/8h) - (2h/d)} \quad (3.8)$$

The equation of the aperture area may also be expressed in terms of focal length and rim angle as [Stine and Geyer, 2001]

$$A_a = 4\pi f^2 \frac{\sin^2 \phi_r}{(1 + \cos \phi_r)^2} \quad (3.9)$$

3.2.2 Reflection of energy to the receiver: Focal flux distribution

The dish reflector can be composed by continuous smooth mirror or by tiles. The tiles can either be mounted individually or grouped to form a reflector unit. The focal flux distributions in a reflector surface composed for grouped tiles are similar to those having continuous smooth mirror with about the same surface slope errors [Johnston et al, 2003]. In the reflector composed by tiles mounted individually, the distribution of solar radiation in each flat tile is a cone with a Gaussian directional distribution [Timinger et al, 2000]. However, the flux distribution in focal plane is a function of position of mirrors in the reflector, which is independent of the arrival direction of the rays. An ideal sharp focus from a paraboloidic dish gives very high radiation fluxes that may be harmful to materials or humans by a malfunctioning of the system. By using tiles, sharp foci are avoided. For the type of systems discussed here, a concentration factor exceeding 100 is not desirable.

3.2.3 Tracking mechanism

The concentrator must be orientated directly at the sun with angle of incidence of irradiation close to zero. The amount of rotation required to do this orientation is called the tracking angle, which depends on the position of the sun in the sky. If the collector aperture is not oriented well to the sun, some of energy that could be collected is lost. Two types of tracking mechanisms are used: the polar tracking and azimuth/elevation tracking.

In the *polar tracking* systems, the main axis of rotation is aligned parallel to the earth axis of rotation (polar axis). The alignment gives the concentrator a tilt from the horizon equal to the local latitude angle ϕ . The tracking angle about the polar axis is the sun hour angle ω . The other axis of rotation which is perpendicular to the polar axis, the tracking angle is the declination angle δ . The sum of the declination angle and the latitude is equal to the complement of solar midday height.

For *azimuth* or *elevation tracking* the collector aperture must be free to rotate about the zenith axis which is the solar azimuth angle γ_s and an axis parallel to the earth surface. The tracking angle about the horizontal axis is the solar altitude angle α .

The polar mount for low tech system is more recommendable since the controlled rotation is necessary only around one axis. Declination changes less than 0.5° per day, which may be done manually.

Chapter 4

Description and Construction of the System

This chapter provides a detailed description of the system as well as presents all experimental methods and procedures of the work done.

4.1 General

The complete system includes: the concentrator, the receiver and a thermal storage, which is illustrated in Figure 4.1.

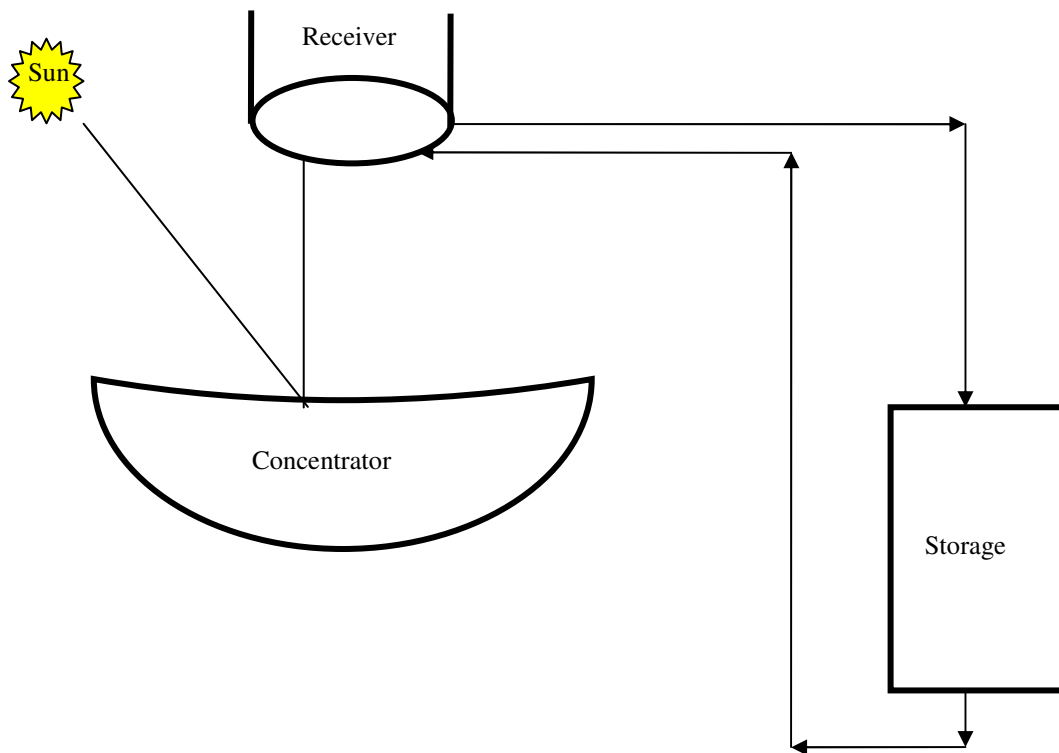


Figure 4.1: Diagram illustrating the components of the system.

The general idea of the system is to pump the cold fluid from the storage to the receiver where it absorbs the heat. The hot fluid from the receiver is pumped to charge a heat storage system, and the cycle continues. This thermal storage system is reported by Mawire [2005], where a solar radiation concentrator/collector was simulated using an electrical hot plate. The entire structure carrying the concentrating collector (polar tracking system) illustrated in Figure 4.15 was designed by van den Heetkamp. In this work the solar radiation concentrator was constructed to replace the electrical hot plate as well as the appropriate receiver for the concentrator. Since the concentrating collector is made to track the sun, some of the pipes connecting the receiver to the storage were replaced by flexible hoses. The remaining pipes are a pair of length 0.6 m, connected to the storage. These pipes are made of copper material, with internal diameter of 4 mm. These pipes were not changed to avoid rebuilding the storage, which was not the aim of the current project

4.1.1 The concentrator design and construction

a) Design

The half-dish concentrator consists of grouped tiles fixed on aluminum frame of satellite communication dish of 2400 mm aperture diameter. The entire frame satellite dish is divided in 6 sectors “petals”. Three petals correspond to the half-dish.

The half-dish frame supports 447 tiles of approximately 80 mm height. The height is reduced from the vertex of the concentrator towards the rim (Table 4.1). The height of the tiles was chosen to achieve an adequate size and number of tiles. Small size is preferred in order to ensure a good parabolic shape. However, very small tiles can decrease the efficiency of concentrator and make the construction excessively cumbersome.

The number of tiles to cover the half-dish concentrator and their sizes were calculated for each petal, being 149 tiles divided in 15 rings; each ring consists of a certain number, and dimension of tiles, depending on its position (Table 4.1). The tiles are trapezoidal, which

is more convenient to the petal design. The number of tiles in each ring and their dimensions were calculated using a Matlab programme developed by Professor Jørgen Løvseth. Table 4.1 shows the dimensions of the tiles: the number of mirrors per ring, the dimensions of lower side and upper side of the tiles, the angles of the tiles, the outer and the inner radius of the ring. The inner and outer radius allows determining the height of the tiles and the gaps between them.

Table 4.1: Dimensions of the elementary mirror in the reflecting surface for each ring.

Ring no. for petal	No. of small mirrors for ring	Dimensions of upper side of tile (meters)	Dimensions of lower side of tile (meters)	Angle of tile (degree)	Outer Radius of the ring (meters)	Inner Radius of the ring (meters)
1	3	0.0727	0.0451	10.0000	0.2093	0.1300
2	4	0.0756	0.0551	7.5000	0.2894	0.2111
3	5	0.0770	0.0608	6.0000	0.3684	0.2910
4	6	0.0778	0.0645	5.0000	0.4462	0.3697
5	7	0.0782	0.0669	4.2857	0.5229	0.4474
6	8	0.0783	0.0685	3.7500	0.5984	0.5240
7	9	0.0782	0.0697	3.3333	0.6726	0.5993
8	10	0.0780	0.0705	3.0000	0.7455	0.6734
9	11	0.0778	0.0710	2.7273	0.8171	0.7663
10	12	0.0774	0.0713	2.5000	0.8874	0.8178
11	13	0.0770	0.0715	2.3077	0.9564	0.8881
12	14	0.0766	0.0716	2.1429	1.0241	0.9570
13	15	0.0761	0.0715	2.0000	1.0905	1.0246
14	15	0.0763	0.0716	1.8750	1.1556	1.0910
15	16	0.0798	0.0757	1.8750	1.2196	1.1561

b) Construction

The materials used to construct the half dish concentrator are: trapezoidal tiles, clear silicone sealant, and half satellite communication dish (made up of three petals).

The tiles are made up of acrylic mirror material of 2 mm of thickness, since it is available at reasonable cost. Acrylic mirror has reflectance of 87%. The total area of the mirror required to cover the full dish surface was 2850 mm². A maximum standard width of continuous acrylic mirror found is 2400 x 1200 mm, which was cut into individual tiles using a laser by the Lasercore Company.

The greatest problem in the construction of the dish concentrator is to get a good parabolic shape, due to the paraboloidal curvature. This was one of the reasons to use acrylic mirror, since is a little more flexible than glass which is more affordable. In the construction of the half-dish concentrator, the silicone glue was used to fix the trapezoidal tiles in the satellite dish frame. Between the tiles there are gaps of a few millimeters to avoid overlap of the tiles. These gaps were carefully covered by silicone to protect the mirror from environment degradation and corrosion.

4.1.2 The receiver

In terms of configuration, receivers can be flat receivers or cavity receivers. Flat receivers are focal absorber surfaces whilst cavity receivers (three- dimensional) have the absorber surface surrounded by an insulated glass cover, with a sufficient opening to capture the radiation from the concentrator. The opening must be as small as possible to avoid losses. The shape of the receiver depends on its dimension and the concentrator focal length/rim angle. Since the rays of the sun that reach the concentrator are not parallel due to the finite angular size of the sun's disc [Stine and Geyer, 2001] and the parabolic dish surface not being ideal, the distribution of reflected rays across the focus forms an image of finite size centered about the focus, instead of a point, as supposed. The image produced will determine the receiver size. Appropriate dimensions of the image can be calculated for perfect and imperfect parabolic concentrators. Here, the dimensions of the receiver were obtained using two different experimental methods: by scanning a reflector using a laser

beam system and by scanning the temperature profile on the back side of a thin stainless steel plate used as a solar flux indicator.

a) Determination of focal length and receiver dimensions

Laser scan

Figure 4.2 illustrate the laser measurement scheme. The main component of the optical scheme is the scanner consisting of a Dewalt laser DW082K. The scanner is fixed in a support frame which allows the light beam to scan different sections of the petal. The scanner (laser beam) will hit the mirrors, each petal, one by one. The petals are fixed horizontally with a slightly elevation of about 390 mm in the rim. This elevation corresponds to the height of the full parabolic dish in question. The light beam incident in the petal is reflected to the screen which is a square (300 x 300 mm) made of glass. The screen is placed in focal plane in horizontal position. The experiment was also done with the screen in a vertical position.

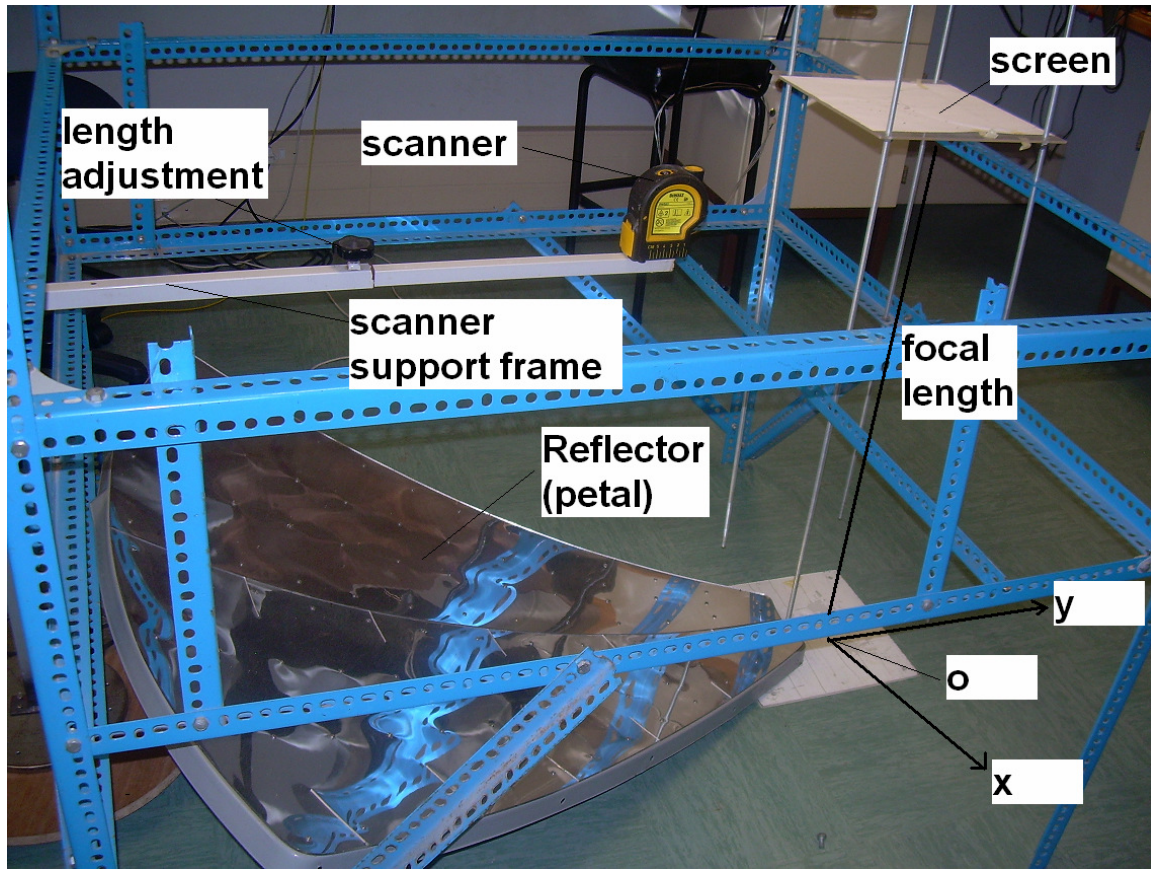


Figure 4.2: The laser measurement scheme with screen placed in focal plane in horizontal position.

A white sheet of paper was placed over the screen where the distribution of reflected points was marked. Often, the boundaries of the images produced by the reflected light across the focus are not well defined. This is due to the slope errors of the concentrator surface. As result, images across focus can be too large. In this case it is better to use a receiver that will not intercept all of the reflected radiation, since is more advantageous to decrease the receiver size increasing optical losses, than to use receivers too large and increase thermal losses. Solar receivers with 5 to 10% of optical losses are acceptable [Duffie and Beckman, 1991]. The receiver dimensions can also be optimized by increasing the focal length of the concentrator and consequently to decrease the rim angle. However in the laser scan method, different focal distances were experimented until the more acceptable was found in order to reduce the receiver size and also capture a large amount of reflected radiation. In our case, this became possible by using a focal length of 994 mm for 100 mm of receiver radius.

The capture fraction (“spillage”) for this receiver radius was calculated considering the following approximation given by equation (4.1) as

$$\%_{\text{losses}} = \frac{\text{nr}_{\text{losses}} * 100\%}{\text{nr}_{\text{tiles}}} \quad (4.1)$$

where $\text{nr}_{\text{losses}}$ is number of losses (being one per tile), nr_{tiles} is the number of tiles.

The percentage of losses for this approximation is about 3.32%, which according with Duffie and Beckman [1991] is acceptable. Figure 4.3 shows the distribution of reflected light across focus at 994 mm of focal length.

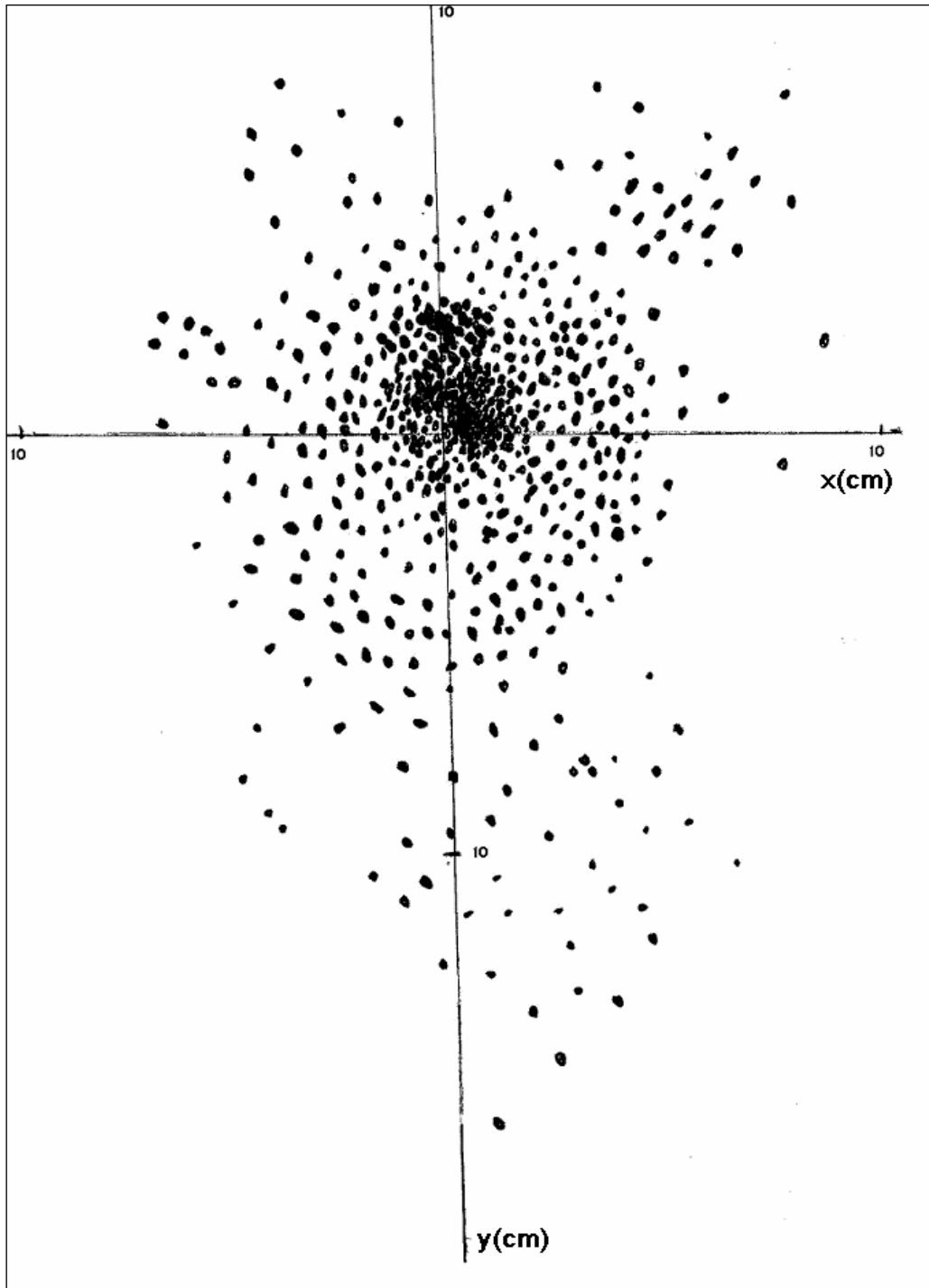


Figure 4.3: Distribution of reflected points

Since the laser measurement scheme evaluates petal by petal, to make sure the receiver dimensions and the concentrator focal length for all petals together (a half-dish) tracked

to the sun, a flat plate of stainless steel was used as solar flux indicator. For that the concentrator was installed with the stainless steel plate as receiver.

Solar radiation

The stainless steel plate was positioned normal to the optical axis at a set of points in the focal area (Figure 4.4). The stainless steel plate must be oxidized at high temperature in an oven. If necessary, a coating of Cr-Ni oxides should be applied first. The aim is to get a thick and stable black oxide layer that is reasonably stable if heated to 700° C, which is the approximate equilibrium temperature at 1 kW/m² sun and a concentrating factor of 100 [van den Heetkamp, 2007].

For a thin plate (1 mm or less) the radial temperature transport is negligible. The profile of the temperature distribution in different radius of the plate was scanned using I-R Gun.



Figure 4.4: Illustration of the stainless steel plate placed at focus.

The temperature scan, besides estimating the receiver radius and the concentrator focal length, allows also verifying the heat distribution onto the receiver area and determines

the receiver configuration. With no hot spots, a flat receiver may be used. Otherwise a cup receiver would be necessary for the system. On the other hand, a trade off between focal length and receiver dimensions is inevitable. According to Kaushika and Reddy [2000], a cavity receiver (three-dimensional) has been suggested for applications in low cost dishes of short focal length ($\phi_r \approx 90^\circ$), since concentrators with a large focal length have a lot amount of spreading of rays to the receiver. In our case, fortunately there were no hot spots, since the focal length of the concentrator (1000 mm) and the radius of the receiver (250 mm) was large to be a cavity receiver. However, a better choice was a focal absorber (flat receiver). Figure 4.5 shows the temperature profile on the stainless. The temperatures are high in center decreasing with increasing radius.

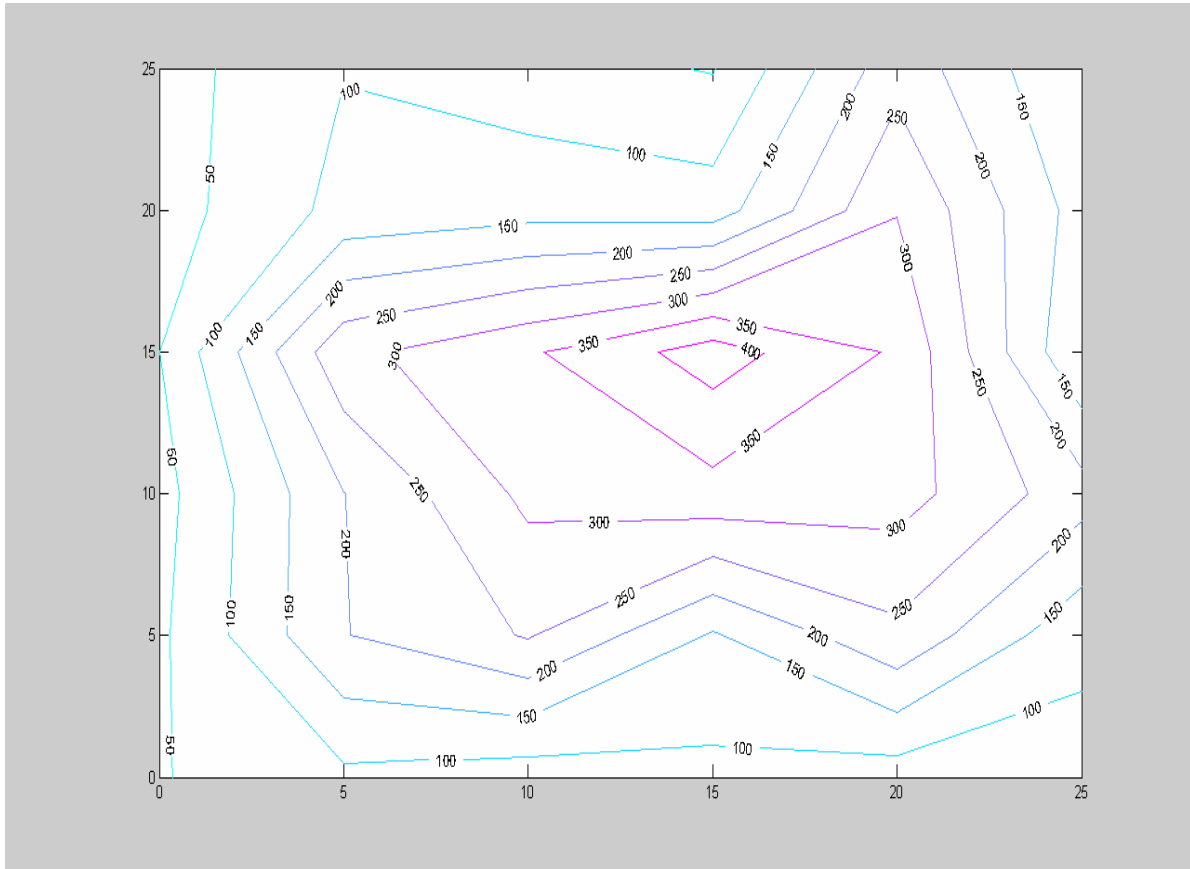


Figure 4.5: Temperature profile on stainless steel plate.

The results of the solar radiation experimental method are more reliable than the results of the laser experimental method, since the dimensions of the receiver and the focal

length of the concentrator using the solar radiation method are determined having in account also the tracking errors of the concentrator. Tracking errors may be small. The laser testing is done petal by petal. The solar radiation testing is done for the mounted petals. Mounting errors may be quite large.

b) Receiver design and construction

The receiver is made up of a stainless steel coil rolled into a spiral shape of diameter 250 mm (Figure 4.6), protected by surrounding box for insulation (Figure 4.8). Copper is a metal with greater heat conductivity than stainless steel, but it oxidizes the oil catalytically. Aluminum is cheap but can melt. This type of receiver is discussed by Kaneff (1995). Usually in this type of receiver the liquid is circulated inside the tube, entering from the rim and leaves at the center where the radiation intensity and temperature is higher. The pipe was enrolled into a spiral shape by Coil Company.

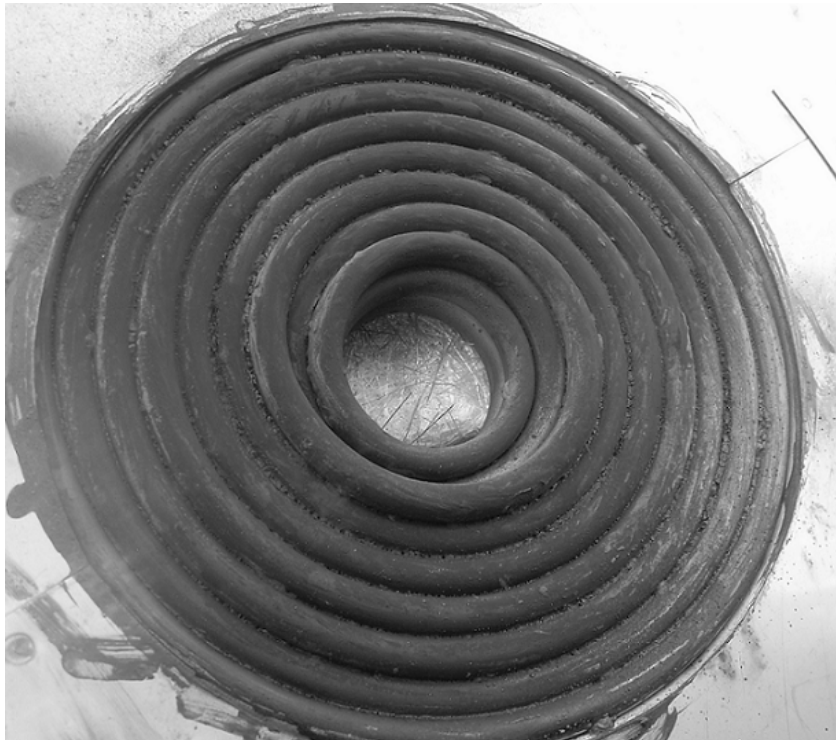


Figure 4.6: The side of solar exposure of the receiver.

It was impossible to bend the pipe into a very small spiral radius as desired (Figure 4.7). To avoid pipe deformations, the receiver has a small hole in the center, of about 40 mm.

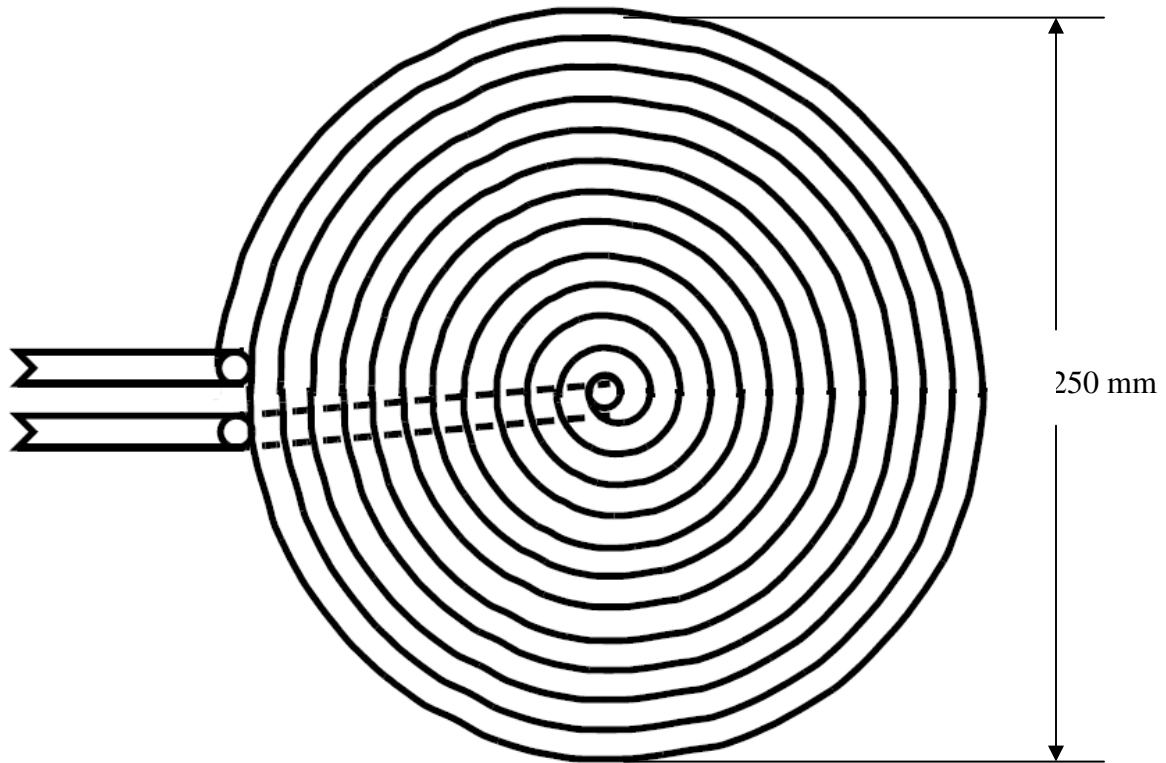


Figure 4.7: Sketch of the receiver.

The coil is painted black (using solvalit heat resistant paint) on the side of solar exposure to increase the absorbance of solar radiation. The coil is protected by a surrounding box. This box is also for insulation. The dimensions of the box are such as to give an insulation thickness of at least 100 mm. The insulation is fiber glass. Figure 4.8 shows photograph of the receiver box.

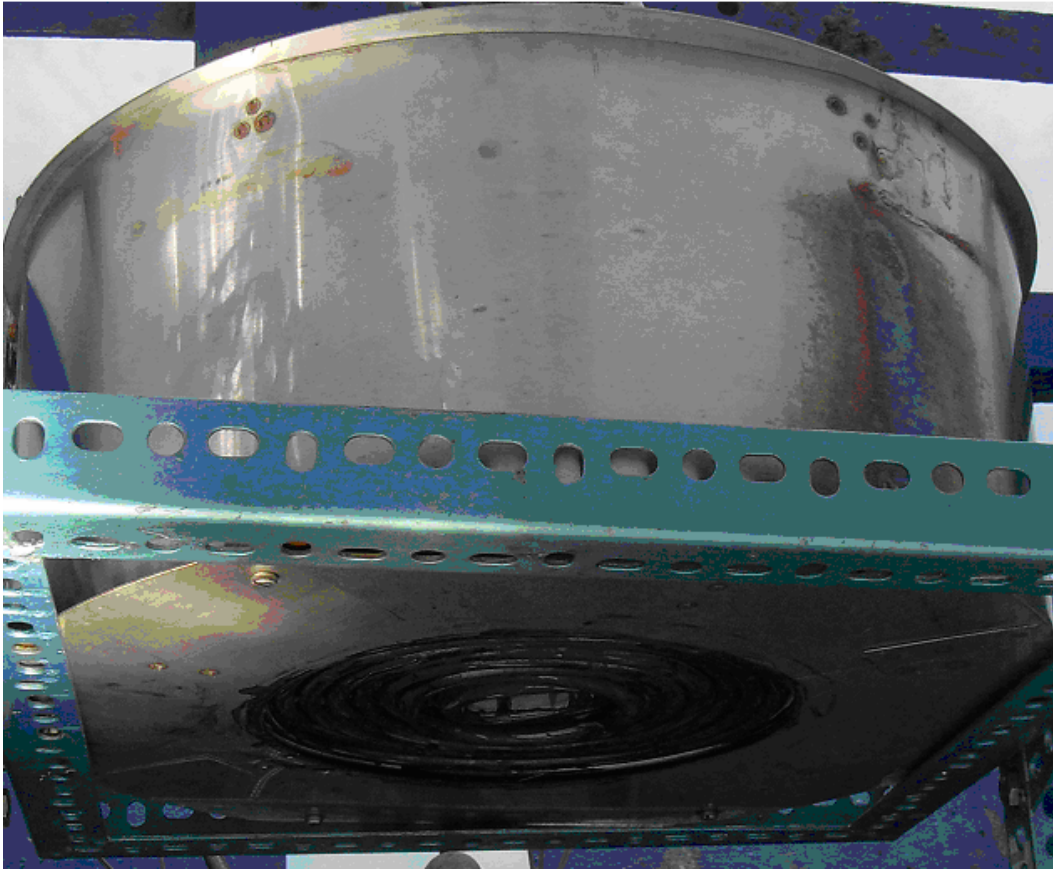


Figure 4.8: Photograph of receiver box

4.1.3 The thermal storage

The thermal storage (Figures 4.9 and 4.10) is a two-phase system that consists of a packed pebble bed made of small sandy stones. The sandy stones are surrounded by the heat transfer oil. Pebble bed storage uses the heat capacity of a packed particulate material to store thermal energy [Duffie and Beckman, 1991]. The fluid that is circulated inside storage through the bed removes and adds thermal energy. This storage was part of study of Mawire [2005].

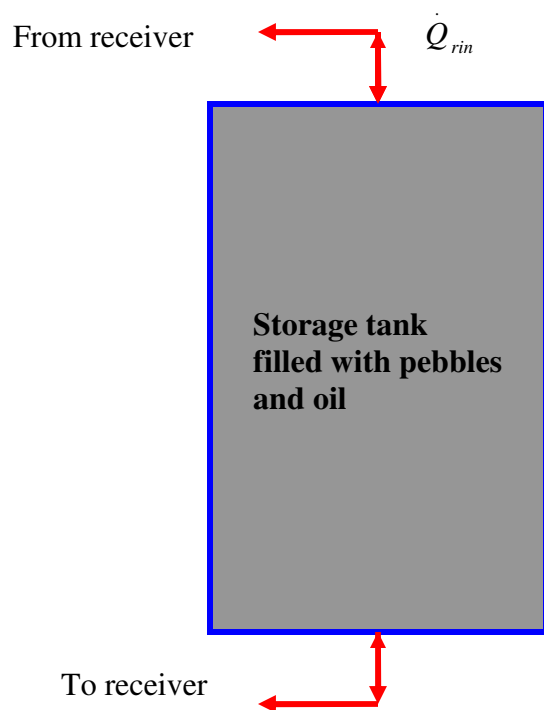


Figure 4.9: The thermal storage diagram



Figure 4.10: Photograph of thermal storage (courtesy of Ole Jørgen Nydal)

4.1.4 The receiver and the heat transfer fluid circuit

The dimension of the pipe (length and diameter) to transfer and transport the fluid is the main parameter to consider, in way to reduce pressure losses caused by the friction of the fluid flow through pipes. The pressure drop increases as the diameter of pipe decreases and is given by [Twidell and Weir, 2006].

$$\Delta P = 4f \left(\frac{L}{D_p} \right) \left(\frac{\rho u^2}{2} \right) \quad (4.2)$$

where f is a pipe friction coefficient depending on surface roughness and the Reynolds number, L is the pipe length and ρ the fluid density. The Reynolds number is defined as:

$$R = \frac{uD_p}{\nu} \quad (4.3)$$

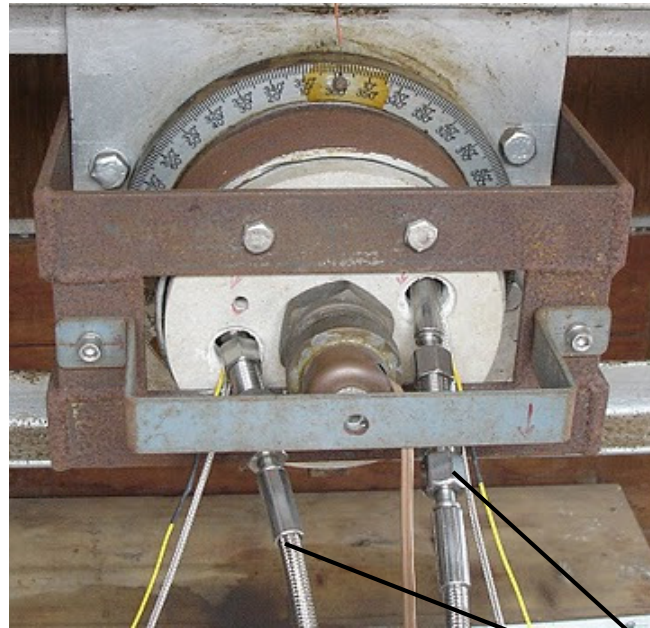
where u is the mean speed of the flow, ν is the liquid viscosity and D_p the pipe diameter. For a given mass flow, the pressure drop increase with D_p .

Based on equation (4.2), pipes with an internal diameter of less than 8 mm give very high pressure loss. This size has been used for the coil itself. Reynolds numbers equal to or higher than 4000 were needed to ensure turbulent flow which was necessary to give sufficient heat transfer without charring of the oil [Lovseth, 2008]. For the transport link 10 mm internal diameter for the PTFE convoluted hoses (Figures 4.11, 4.12 and 4.13) was used. These hoses are flexible to accommodate the polar tracking system, since one set of ends moves with the rotating tracking system and the other set of ends is fixed, and goes to the storage.



Flexible hoses
from receiver

Figure 4.11: Photograph of flexible hoses from receiver (courtesy of Ole Jørgen Nydal)



Flexible hoses
from receiver to
storage

Figure 4.12: Photograph of flexible hoses from receiver to storage (courtesy of Ole Jørgen Nydal)

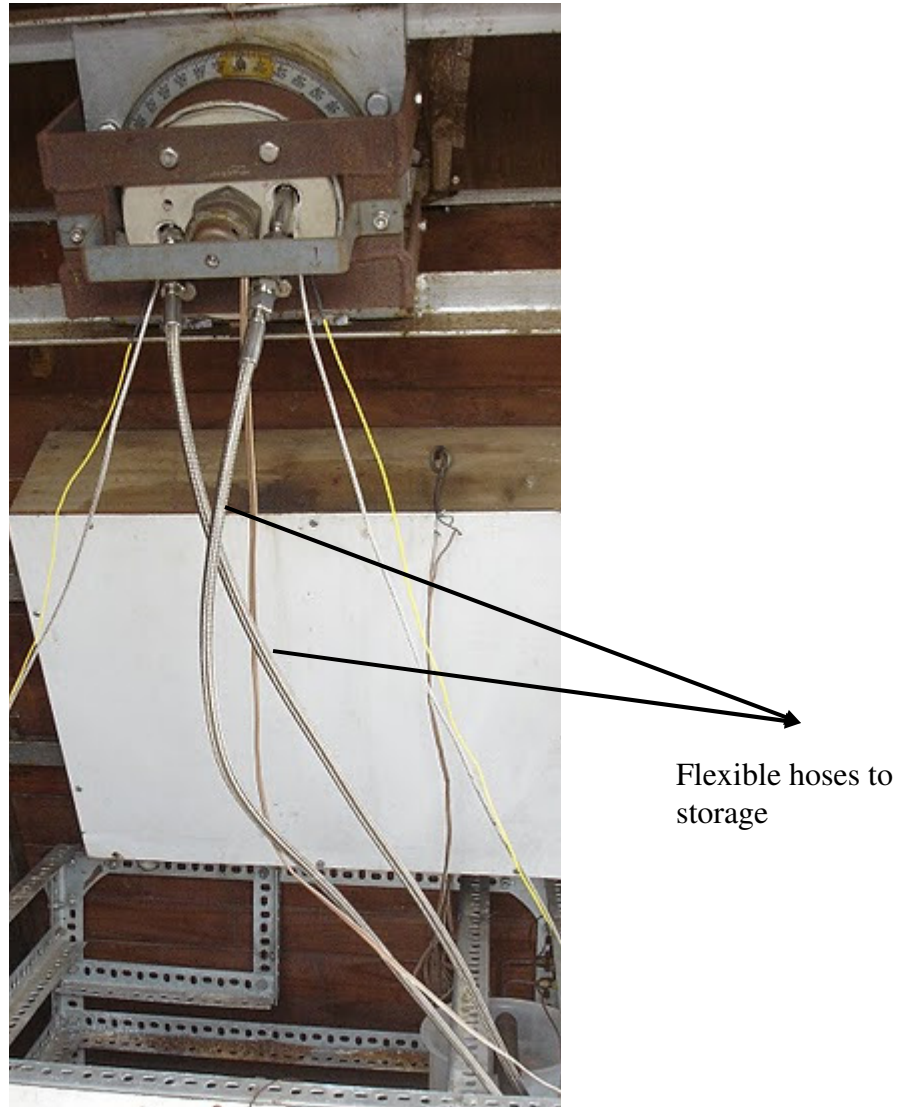


Figure 4.13: Photograph of flexible hoses to storage (courtesy of Ole Jørgen Nydal)

Different fluids can be used, depending on the aim. For our case the main aim was to evaluate the useful energy gain and the heat losses of the system. For that, the density, film coefficient, viscosity and thermal conductivity of the different fluids were studied. Calflo heat transfer fluid was a choice because of negligible vapour pressure and low toxicity. Calflo heat transfer fluid is designed specifically for use in systems operating at temperatures up to 326°C (bulk temperature) [website 2]. Table 4.2 [website 2] shows

the typical performance data of Calflo heat transfer fluid and Table 4.3 [website 2] the thermal data.

Table 4.2: Typical performance data of Calflo heat transfer fluid (source website 2).

Property	Test Method	Results	
Appearance		Crystal Clear	
Maximum Film Temperature, °C		343	-650
Weight/US gal at 260°C,lbs		5.4	
Pour Point, °C(°F)	ASTM D97	< -15	(< 5)
Flash Point, COC, °C(°F)	ASTM D92	226	-439
Fire Point, °C(°F)	ASTM D92	239	-462
Autoignition Temperature, °C (°F)	ASTM E659-78	364	-687
Viscosity, cSt at 40°C(104°F)	ASTM D445	35.6	
cSt at 100°C(212°F)		6	
cSt at 316°C(600°F)		0.73	
Distillation Range, °C (°F)	ASTM D2887		
10%		392	-738
90%		500	-932

Table 4.3: Thermal data of Calflo heat transfer fluid (source website 2).

Property	Temperature			
	38° C (100 F)	204°C (400 F)	260°C (500 F)	316°C (600 F)
Density, g/ml	0.844	0.731	0.694	0.657
Thermal conductivity, W/m K	0.142	0.133	0.13	0.127
Heat capacity, kJ/kg K	1.97	2.51	2.69	2.88
Vapor pressure, kPa	0.00	0.44	2.66	11.44

4.1.5 Pumping process

A flux concentration of 10^5 W/m^2 will provide a flux of approximately $4 \times 10^4 \text{ W/m}^2$ on the tube wall. The temperature gradient in the oil close to the wall with laminar flow is then very high, more than $3 \times 10^5 \text{ K/m}$. Unfortunately, Calflo heat transfer fluid has a low heat conductivity (0.14 W/(mK)), which requires turbulent flow, i.e. $Re > 4000$, at least at high temperature, to mix the surface hot layer into the bulk of fluid. The viscosity is high at low temperatures which require high pump pressure. The pumping power of the Calflo heat transfer fluid for turbulent flow $Re \geq 4000$, $D_p = 10 \text{ mm}$, $L = 8 \text{ m}$ is given in table 4.4 [Lovseth, 2008 ⁽¹⁾]. t_i is the initial temperature, t_f the final temperature, Re the Reynolds number, f the friction coefficient, P the total power pumping, u the velocity, ν the kinematic viscosity, ρ the density and J_m the mass current for various heat inputs.

Table 4.4: Pumping power for Calflo heat transfer fluid (turbulent flow $Re \leq 4000$) [courtesy of Lovseth J, 2008 ⁽¹⁾].

Heat/W	t_i	t_r	Re	f	P/W	u	v	ρ	Jm/g/s
500	50	50.386	4000	0.0531	1745.207	10.04	2.510E-05	830	654.55
1000	50	50.772	4000	0.0531	1745.207	10.04	2.510E-05	830	654.55
2000	50	51.545	4000	0.0531	1745.207	10.04	2.510E-05	830	654.55
500	100	101.555	4000	0.0531	22.872	2.40	6.000E-06	796	150.13
1000	100	103.109	4000	0.0531	22.872	2.40	6.000E-06	796	150.13
2000	100	106.218	4000	0.0531	22.872	2.40	6.000E-06	796	150.13
500	150	153.609	4000	0.0531	1.586	1.00	2.501E-06	762	59.91
1000	150	157.219	4000	0.0531	1.586	1.00	2.501E-06	762	59.91
2000	150	164.438	4000	0.0531	1.586	1.00	2.501E-06	762	59.91
500	200	206.282	4000	0.0531	0.266	0.56	1.400E-06	728	32.04
1000	200	212.564	4000	0.0531	0.266	0.56	1.400E-06	728	32.04
2000	200	220.000	5025	0.0515	0.514	0.70	1.400E-06	728	40.25
500	250	259.068	4000	0.0531	0.079	0.38	9.512E-07	695	20.76
1000	250	268.137	4000	0.0531	0.079	0.38	9.512E-07	695	20.76
2000	250	270.000	7255	0.0493	0.448	0.69	9.512E-07	695	37.65
500	280	290.691	4000	0.0531	0.046	0.32	8.000E-07	675	16.96
1000	280	300.000	4277	0.0526	0.056	0.34	8.000E-07	675	18.13
2000	280	300.000	8553	0.0486	0.419	0.68	8.000E-07	675	36.26

Turbulent flow is enforced. Below 250°C it is difficult to obtain turbulent flow ($Re > 4000$) due to the high kinematic viscosity (ν). Large kinematic viscosity demands large velocity of the fluid, which means large mass flow and a low temperature increase [Lovseth, 2008⁽¹⁾].

4.1.6 Tracking mechanism

The tracking system available is a polar tracking. An automatic tracking has now been made, but was not available at time of measurement. The system was rotated to follow the sun manually. To adjust the tracking system to the right tracking angle a sighting mechanism was used (Figure 4.14).

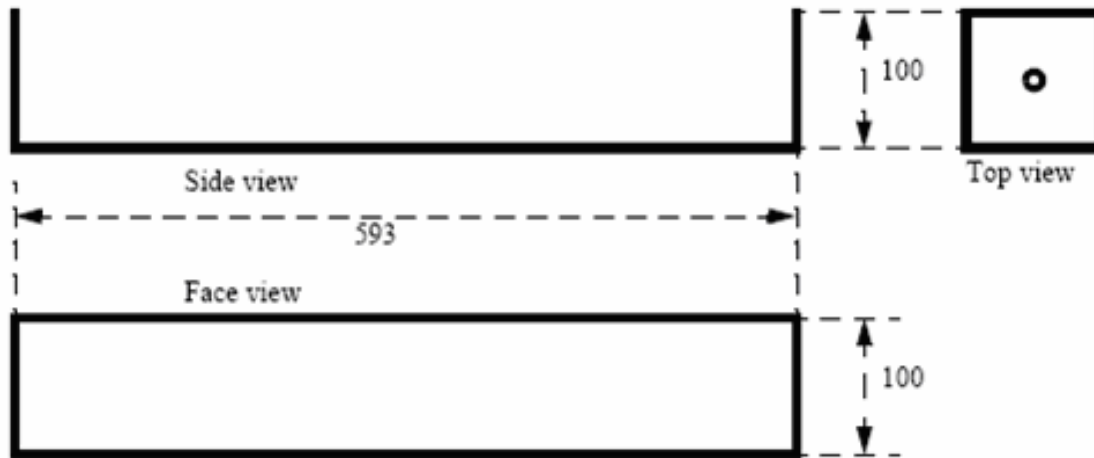


Figure 4.14: The sighting mechanism [courtesy of Lovseth, 2008].

The top flap has a 2 mm hole in the center. The system was focused and a blue dot was marked in the bright spot from the hole. This blue dot is used for tracking adjustment, which means, the system is in the focus when the bright spot is on the blue dot. The distance between the flaps was chosen such that a 1 degree deviation corresponds to 10mm [Lovseth, 2008]. A piece of paper was glued on the lower flap (with rain protection) to indicate deviation from focus in degrees. This was attached to the base frame carrying the parabola (parabola axis).

4.2 Installation of the complete system

4.2.1 Environmental stability

Solar collectors are placed outdoors where they can capture more radiation, usually on the roof of buildings; facing the sun. The place must be free of obstacles that can cause

shadows. To withstand the force imposed by the strong wind, concentrators are usually moved to stowed position. The present parabolic dish collector is placed on the roof of the physics building (Figure 4.15), at University of KwaZulu-Natal, Westville Campus.

The petals were conveniently mounted on a large steel plate attached to the polar tracking system to secure a steady position. The receiver is also attached to the polar tracking system at the focal distance, of one meter from the center of the half dish.



Figure 4.15: The location of solar concentrating collector at University of KwaZulu-Natal.

4.3 Data acquisition

The data acquisition system measured the temperatures of the oil, receiver surface and environment, the charging flow rate and the direct solar radiation. The corresponding diagram is shown in figure 4.16.

For data acquisition a Hewlett Packard (HP) data logger model 34970A (20 channels multiplexer) was used. For data control and display, a data logger was connected to a computer using a Recommended Standard 232 serial port. The software for data operation was Bench Link, downloaded from the internet. The data scan in the data logger was set to read at a time interval of ten seconds. All measurements were taken with the same frequency.

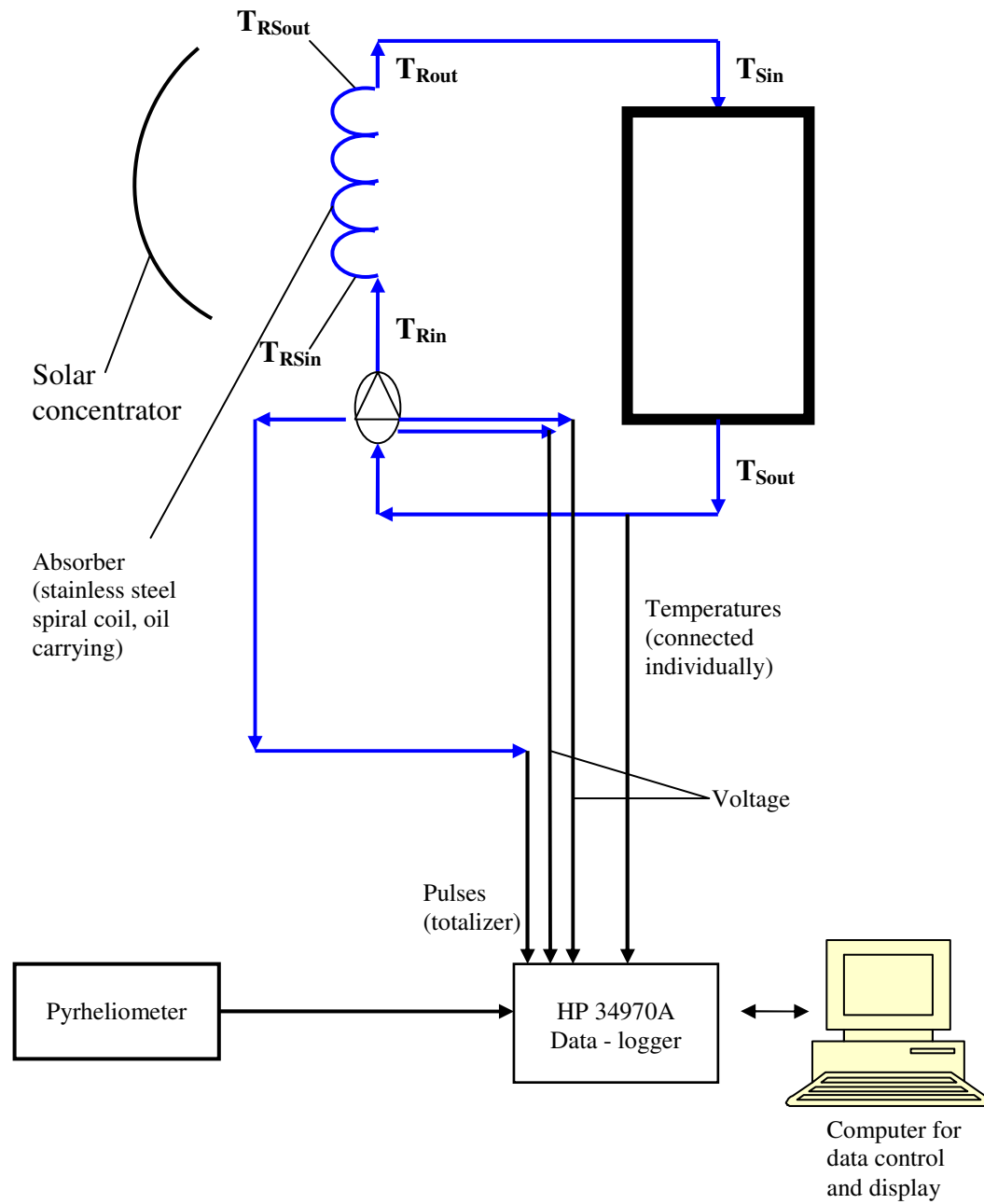


Figure 4.16: The schematic diagram of data acquisition system.

4.3.1 Temperature measurement

Seven temperatures were measured, four for the fluid (two in charging loop and two in discharging loop), two for the receiver surface and the environment temperature. The temperature of the fluid was measured at storage entrance (T_{Sin}) and storage exit (T_{Sout}), at the receiver inlet (T_{Rin}) and the receiver outlet (T_{Rout}). Knowing the temperatures of the oil at receiver outlet and storage inlet the heat losses in the transport of the fluid can be calculated. The temperature of the pipe (receiver surface) was measured at receiver inlet (T_{RSin}) and at receiver outlet (T_{RSout}) in a way to estimate the heat losses between the fluid and the receiver.

The temperatures were measured using K-type thermocouples. This type of thermocouple is composed of chromel and alumel and the temperature range is about -200°C to 1250°C [website 4]. The chromel wire is insulated yellow and is connected to the positive terminal while the alumel wire is insulated red and is connected to the negative terminal of the data-logger multiplexer 37901A.

The data acquisition system was placed relatively close to the solar concentrating system and the connection between them was made by the proper thermocouple of 3.0 meters length in a way to achieve a high precision of the temperature measurement. Each temperature was measured individually in degree Celsius.

4.3.2 Flow rate measurement

A gear pump (Figure 4.17) from a motorbike was used for oil flow. It was connected between the storage outlet and the receiver inlet. To determine the flow rate, the same procedure detailed by Mawire [2005] was used. Mawire [2005] used a mouse disk with many slots. In our case we used a disk with only one slot (Figure 4.19). The pump was calibrated to measure the amount of oil that flows per revolution. Knowing the amount of oil that flows per revolution, it is possible to determine the flow rate by measuring the motor rotational speed. The direct current (DC) motor is YB77XL – 2450 – 31 MEH. At maximum efficiency, 9.6 V, the current is of 3.5 A, the Torque 1.1 Kg.cm for Speed

5,563 rpm. This motor was appropriate for the power supply available, for which the maximum current is 5 A.

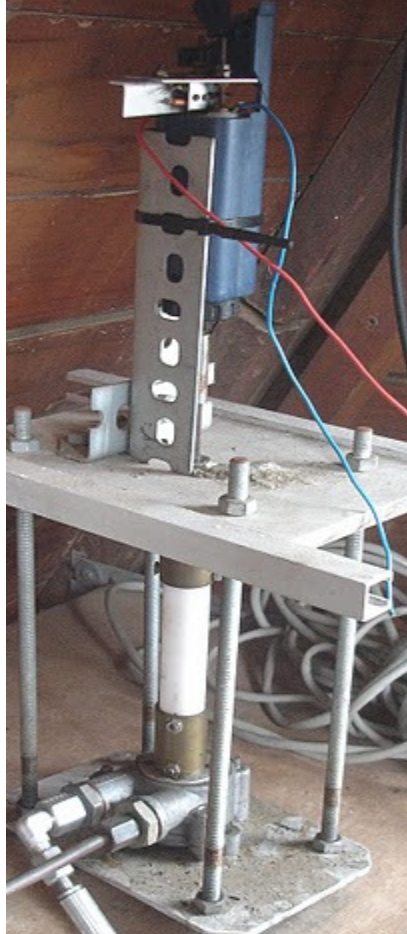


Figure 4.17: Photograph of the pump (courtesy of Ole Jørgen Nydal)

To calculate the volume of the oil flowing per revolution the pump was used to circulate the fluid during a period of time. An optical switch and a disk with one slot were used to count the pump revolutions. The optical switch comprises a diode which emits infrared light and a photo-resistor which detects the infrared light. The circuitry of the optical switch is illustrated in Figure 4.18.

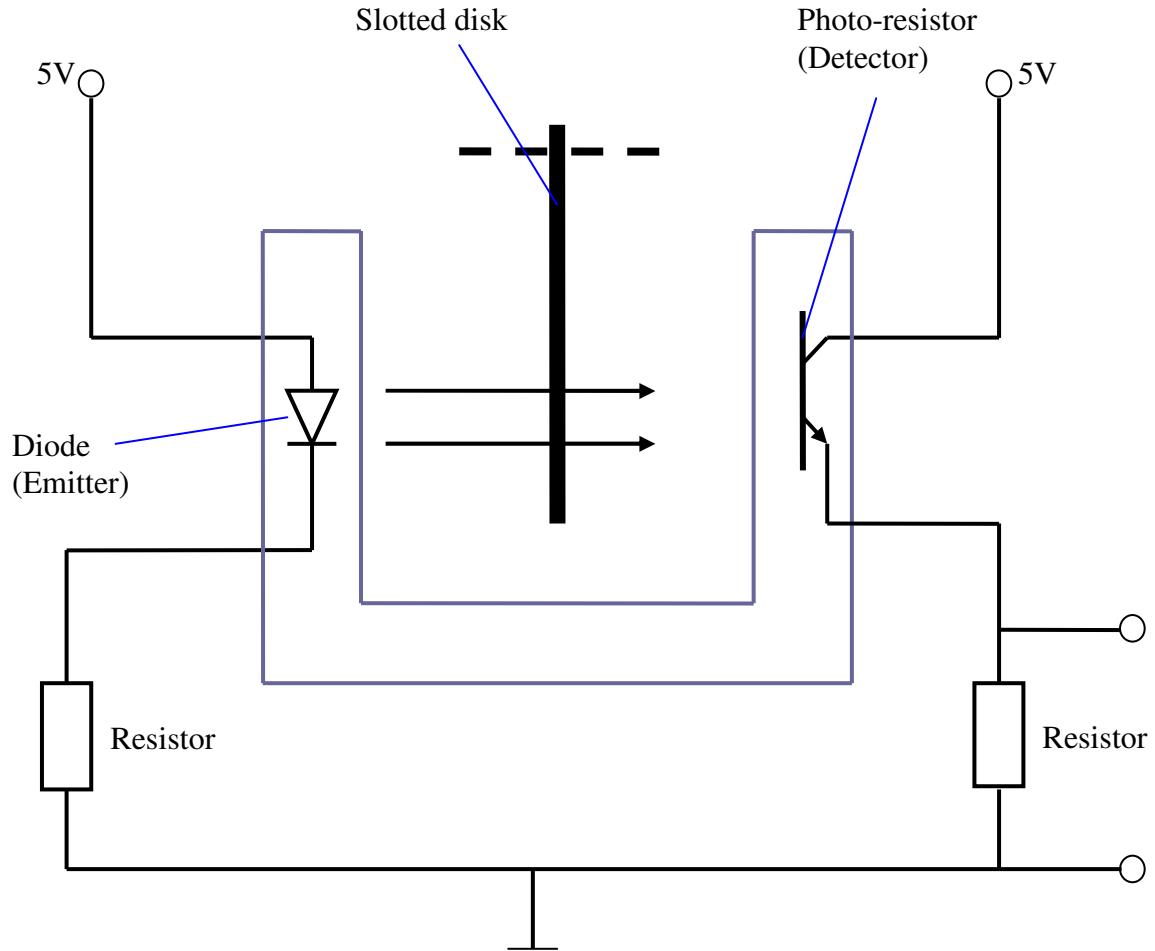


Figure 4.18: The circuitry of optical switch.

The slotted disk (Figure 4.19) was made of copper. It was attached to the shaft of the motor, and designed to follow the pump rotation (Figure 4.20). The optical switch is attached such that the slotted disk stays in between the infrared light emitting diode and the photo-resistor (the detector) (Figure 4.20).

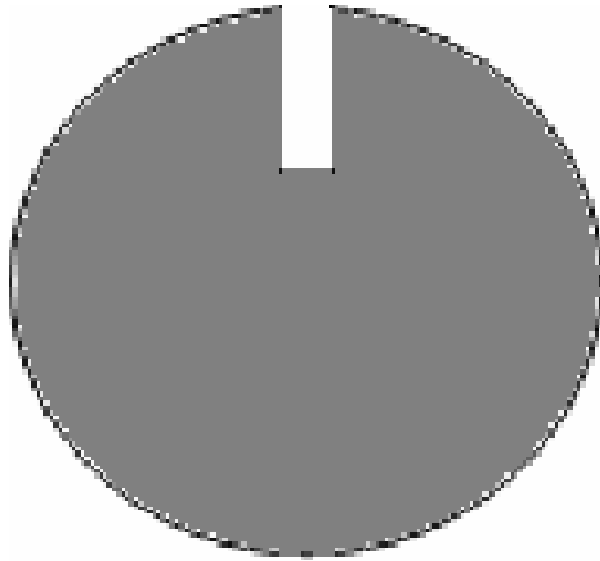


Figure 4.19: Sketch of the slotted disk.

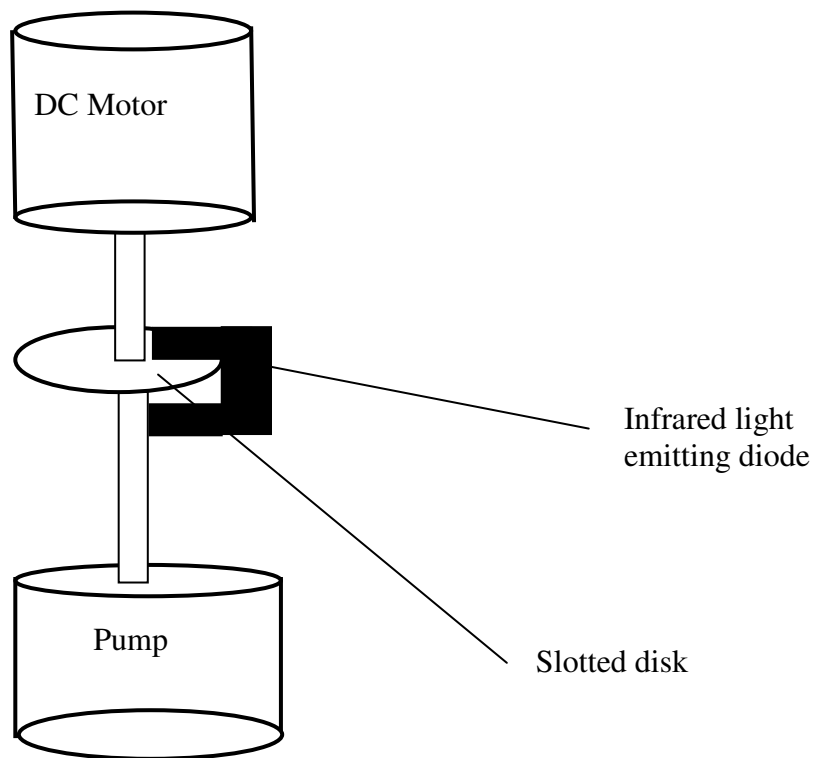


Figure 4.20: The attachment of the optical switch and the slotted disk in the pump.

When the slotted disk rotates with the pump rotation, the infrared light is blocked or detected by the detector. When the infrared light is blocked, there is no passage of current to the resistor, and the output voltage is zero. When the infrared light passes to the detector, the output voltage is about 4.5V (Figure 4.21). This blockage/unblockage of the infrared light creates pulses (square waves) which are totalized for counting using a multifunction modulo 37907A of the data-logger, which has “26-bit totalizer” and can count transistor-transistor logic (TTL) pulses at a rate of 100 kHz [Hewlett Packard, 1997].

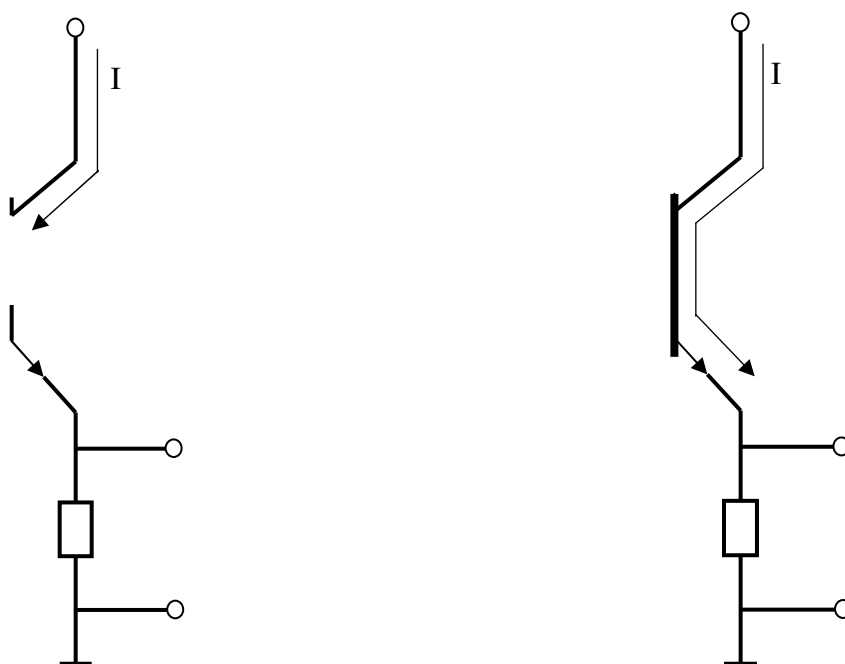


Figure 4.21: The blockage and unblockage of the infrared light.

The pump was used to circulate oil from one graduated container to another graduated container. The optical switch and the slotted disk were used to count the number of revolutions made by the pump during the pumping process. The total number, after a period time was displayed by the data-logger. The amount of oil pumped for the total number of counts in interval of time was recorded.

The volume of the oil flowing per revolution was given by equation (4.4) as

$$V = \frac{V_t}{C} \quad (4.4)$$

where, V_t is the total volume of the oil pumped and C is the total number of revolutions. The value found in this experiment is 6.10 ml/rev.

After pump calibration, the same optical switch and a slotted disk was used to measure the flow rate. Knowing the number of revolutions during an interval time, the rotational speed of pump can be calculated as

$$R_p = \frac{C}{\Delta t} \quad (4.5)$$

where, C is the total number of revolutions and Δt is the interval of time. The volume of the oil flowing per interval of time during the pumping process is given by equation (4.6) as

$$\dot{V}_f = R_p * 6.10 \text{ ml / rev} \quad (4.6)$$

The mass flow-rate is given by the following equation as

$$\dot{m} = \dot{V}_f * \rho \quad (4.7)$$

where ρ is the density of the fluid.

4.3.3 Direct solar radiation measurement

The beam solar radiation was measured by an Eppley Normal Incidence Pyrheliometer mounted in two axis sun tracking system (Figure 4.22). The direct solar radiation was monitored using the same data acquisition system. This pyrheliometer was connected to the data-logger by using an extension cable. The data from the pyrheliometer were

displayed in volts, which was converted to watt per square meter by dividing the voltage by the factor $7.58 \times 10^{-6} \text{ V/wm}^{-2}$ (pyrheliometer data).



Figure 4.22: The Eppley Normal Incidence Pyrheliometer.

4.4 Efficiency of the solar radiation concentrating system

Energy efficiency of the solar radiation concentrating collector is the ratio between the thermal energy gain and the amount of solar radiation falling inside concentrator. This can be evaluated by knowing the useful energy gain by the system and the intensity of direct solar radiation. It is also important to know the heat losses of the system to improve the efficiency.

The useful energy gain can be expressed mathematically by equation (4.8) as

$$Q_u = \dot{m}c_p(T_{out} - T_{in}) \quad (4.8)$$

Where \dot{m} is the mass flow rate of heat transfer fluid, c_p , the specific heat of heat transfer fluid, T_{out} , the temperature of heat transfer fluid leaving the absorber and T_{in} , the temperature of heat transfer fluid entering the absorber.

The thermal efficiency of the system can be written as

$$\eta = \frac{Q_u}{Q_{beam,in}} \quad (4.9)$$

where $Q_{beam,in}$ is the direct solar radiation input. The solar input is given by equation (4.10) as

$$Q_{beam,in} = I_b A_a \quad (4.10)$$

where, I_b is the direct solar radiation and A_a the area of the concentrator aperture.

Radiation losses may be dominant for concentrating systems. Radiation losses are transfer of heat through space, by electromagnetic waves. The rate of radiation heat losses depends of the receiver material, since it is proportional to the emittance of the surface. The radiation losses are also proportional to the difference in temperature to the fourth power and the receiver area. Mathematically, this can be described by equation (4.11) as

$$\dot{Q}_{loss,radiation} = \varepsilon \sigma A_r (T_r^4 - T_{sky}^4) \quad (4.11)$$

where ε is the emittance of the receiver/absorber surface, σ is the Stefan – Boltzmann constant ($5.670 \times 10^{-8} \text{ W/m}^2\text{K}^4$) and T_{sky} is the equivalent black body temperature of the sky.

Chapter 5

Results and discussion

The major part of the data was collected in clear sky days. This is because it was an objective to find the maximum efficiency of the system. Data of five days with clear sky are presented in the Figures 5.1.1.a,b,c,d,e,f; 5.2.a,b,c,d,e; 5.3.a,b,c,d,e and 5.4.a,b,c.

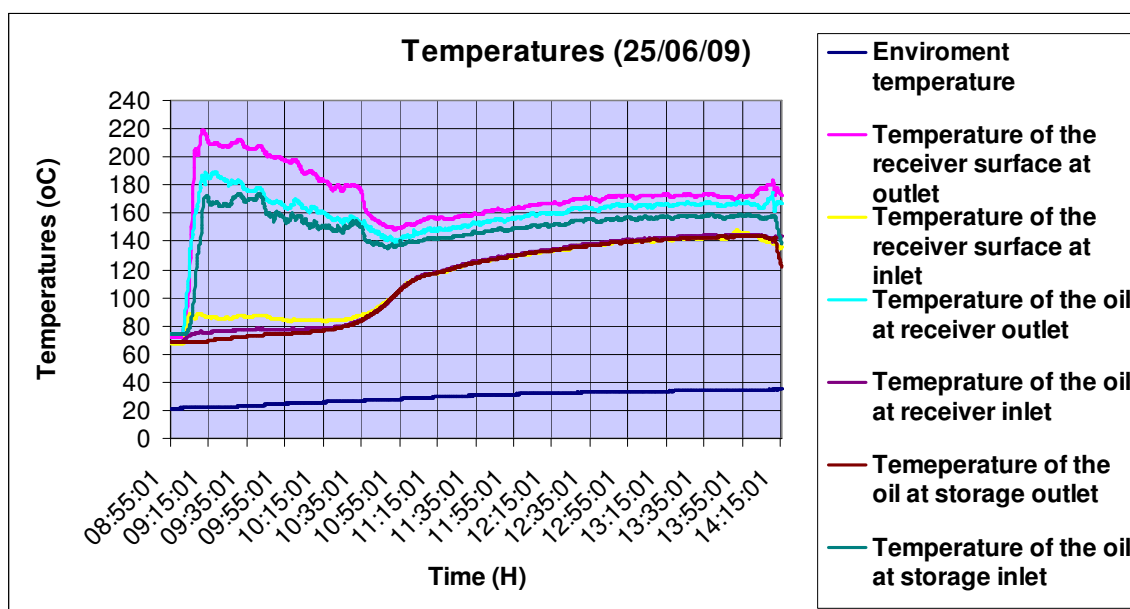


Figure 5.1.a: Results of temperatures measurements, on 25th June, 2009.

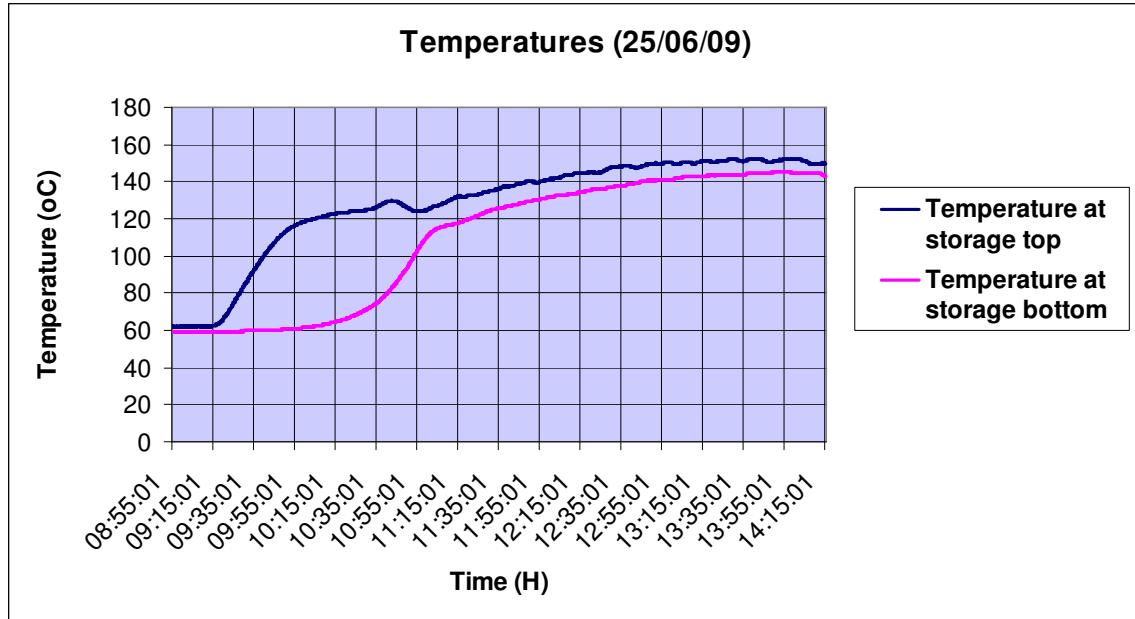


Figure 5.1.b: Results of temperatures measurements inside storage, on 25th June, 2009.

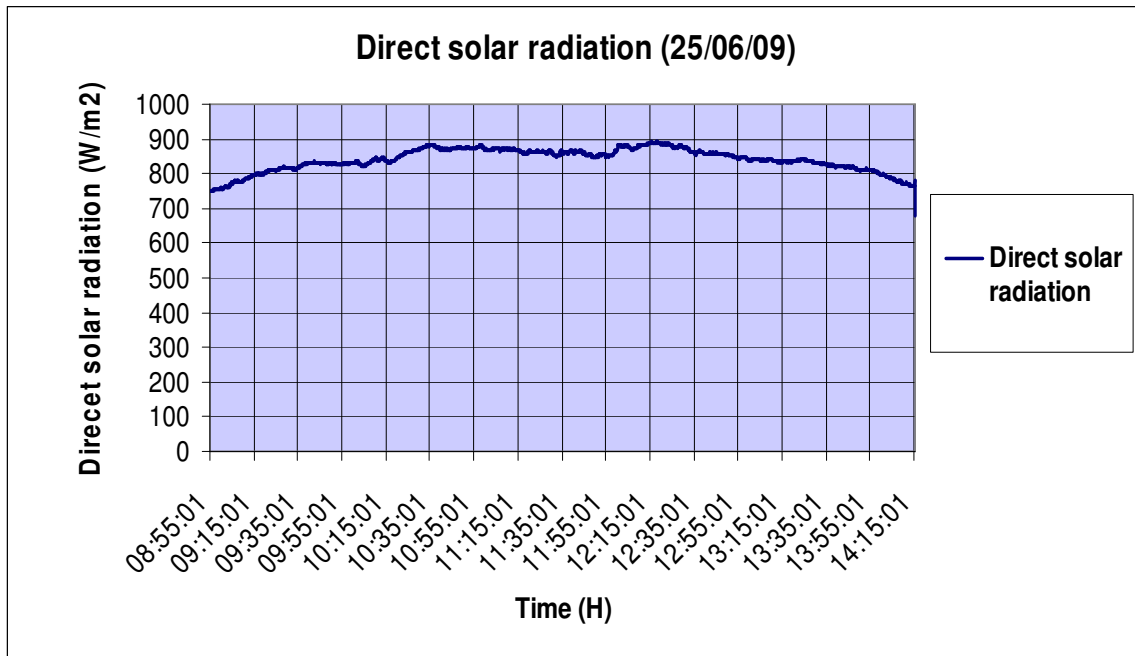


Figure 5.1.c: Results of direct solar radiations measurements, on 25th June, 2009.

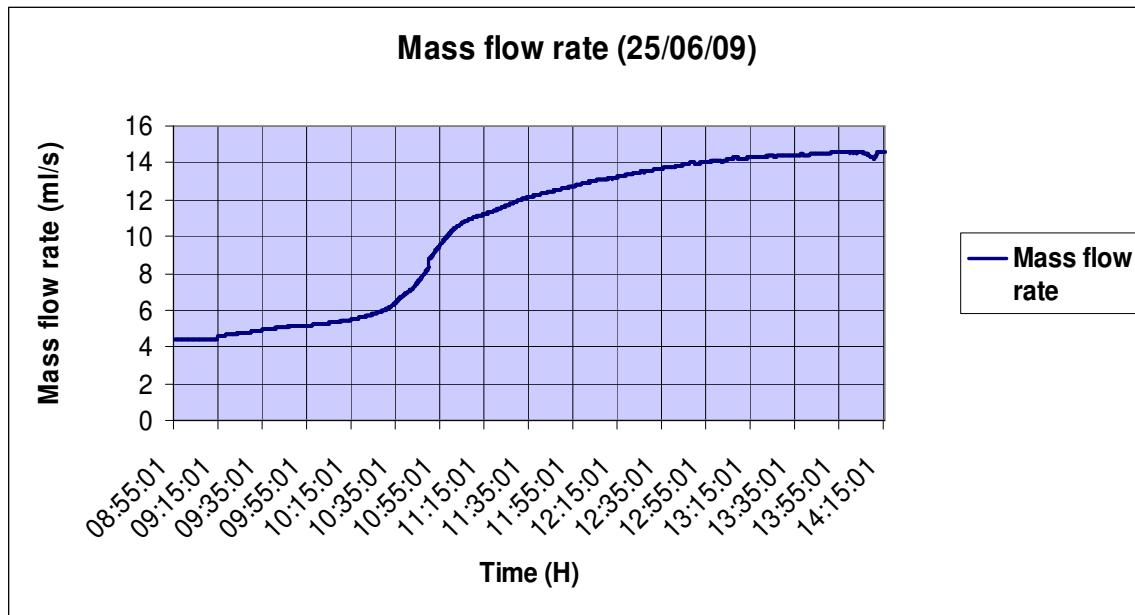


Figure 5.1.d: Results of mass flow rate measurements, on 25th June, 2009.

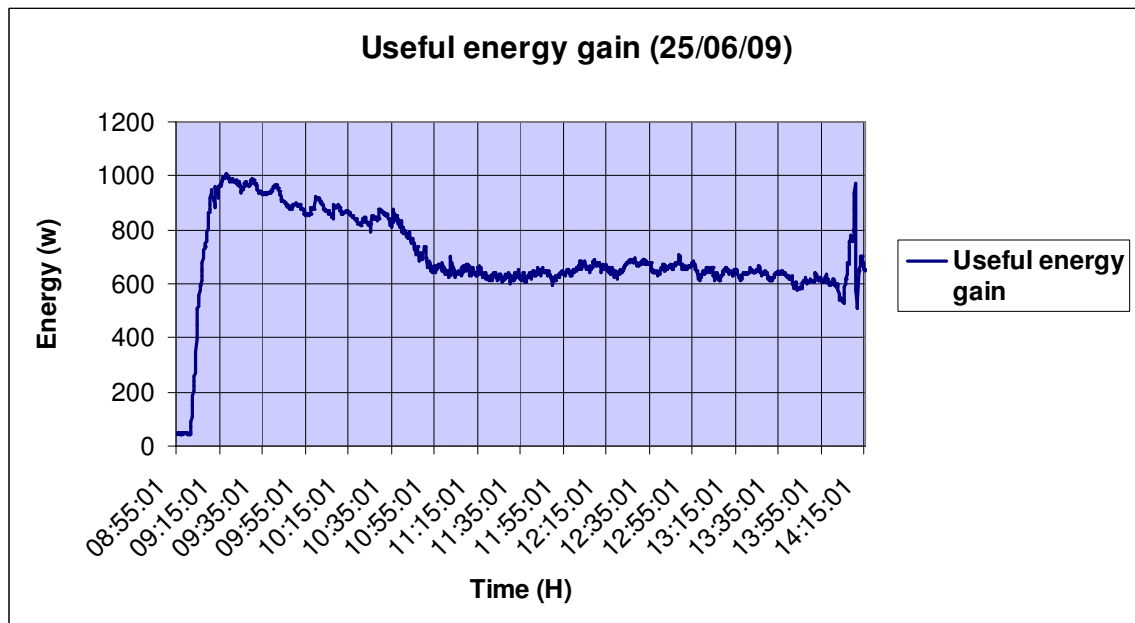


Figure 5.1.e: Useful energy gain on 25th June, 2009.

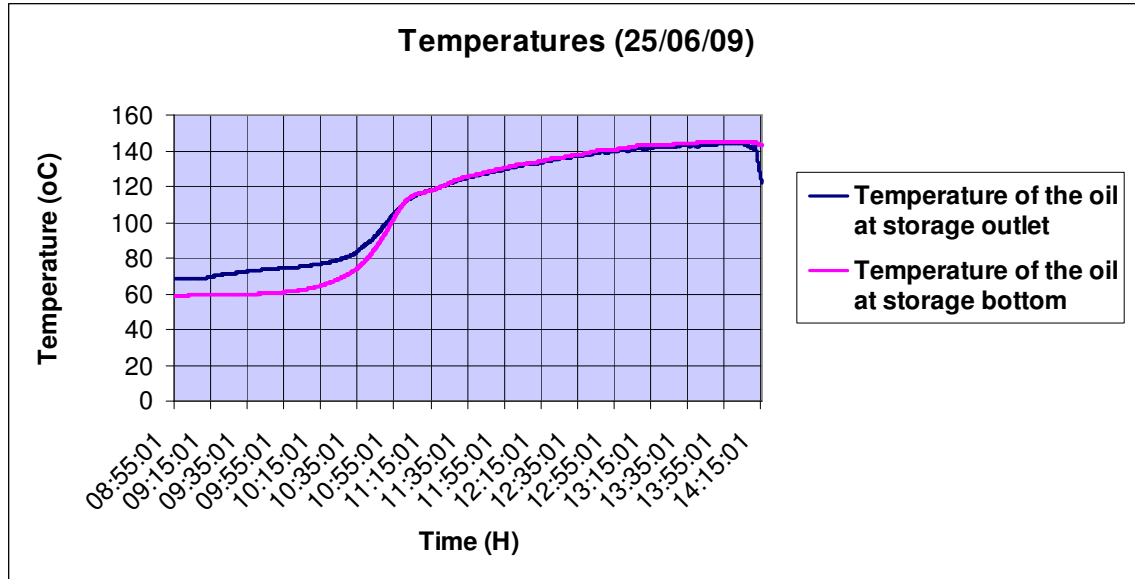


Figure 5.1.f: Temperature of the oil at storage outlet and at storage bottom on 25th June, 2009.

In figures 5.1.a and 5.1.b temperatures are high from 09:15 hours to 10:35 hours, decreasing at 10:55:01 hours. This behavior in the temperatures can be due to the pump. The pump probably has an internal leakage and requires more pumping pressure to circulate sufficient oil when the oil is cold.

Initially there is a long temperature gradient across the storage, with highest temperature at the top and lowest temperature at the bottom. As the storage becomes fully charged this gradient decreases. Then the entire storage tends to follow the temperature of the incoming fluid due to high pumping rate. This can be seen in figure 5.1.b; the temperature difference between inlet and outlet after 11:15:01 is in order of 10 degrees and before this time is higher.

The flow rate increases by factor 6 at 10:55:01 hours. The reduced oil flow in the initial phase is due to high oil viscosity, table 4.4, which indicate that the pump will not function until a temperature between 100 and 150°C. The maximum power to the pump is some 34 W, but probably is far off the all optimal work point, and therefore has a low efficiency. The initial large gap between temperature on receiver surface and oil at outlet is an indication of this; heat transfer to the oil is inadequate.

This temperature difference is drastically reduced as soon as inlet oil to the receiver passes 100°C. The temperature increase of oil is however slow after this point, which is due to bad insulation of the storage (refurbishment of the storage was not part of this project).

The temperature of the oil at storage outlet is higher than the temperature of the oil at the storage bottom at the beginning of pumping process. This is due to the heat exchange between the inlet storage pipe and the outlet storage pipe, since they are not insulated from each other. The length of the pipe from the storage outlet to where the thermocouples are connected is about 0.6 meter. The distance between the two pipes is 0.05 meters. These pipes are made of copper material as said in section 4.1. The radial distribution of heat inside storage is also uneven. Figure 5.1.f gives an example of the temperature difference, from 08:55 hours to around 10:55 hours.

After the reduction of temperatures with the increment of oil flow rate, the difference of temperature between the receiver surfaces, the oil at receiver outlet and the oil at storage inlet decrease and become almost constant. The increment of temperature is gradual.

The maximum amount of direct solar radiation achieved was almost 900 W/m² (Figure 5.1.c). This day was characterized by a clear sky day and therefore with less oscillations of solar radiation intensity.

The useful energy gain is directly proportional to the difference of temperature between the temperature of the oil at the outlet and inlet of the receiver. The useful energy gain is in the interval of 700-1000 W from 9:15:01 hours to 10:55:01 hours and near 700 W after this interval as shown in Figure 5.1.e. The useful energy gain was calculated using equation 4.10.

Useful energy gain (Fig. 5.1.e) seems to be high in the first period with insufficient oil circulation, when the input oil is heating up. There is no reason for high heat supplied (high efficiency) in the morning than in the afternoon since the receiver surface at outlet

is higher in the first two hours. This is probably to the pump leakage (bad flow) as the flow resistance is very high in the morning period.

Considering heat capacity of the storage $C_s = 36.8 \text{ kJ/K}$, from Figure 5.1.b, it can be noted that the heating of the storage is at $\Delta T = 60 \text{ K}$ in time interval of $\Delta t = 6600 \text{ s}$. The heat absorbed will be: $\Delta Q_A = C_s \Delta T = 2.21 \text{ MJ}$. From Figure 5.1.f it can be estimated that the mean useful energy (heat current) in this charging period was $Q_1 = 900 \text{ W}$. The heat supplied in this interval of time is calculated as $\Delta Q_{In1} = J_{Q1} \Delta t = 5.94 \text{ MJ}$. This is not reasonable. The true value of the heat transfer is probably closer to the value of the oil after this has been heated, because leakage in the pump is higher while the oil is cold and requires high pumping pressure. Taking into account the mean heat current after the oil is heated, $Q_2 = 600 \text{ W}$ is probably more reasonable. With this value the heat will be $\Delta Q_{In2} = 3.96 \text{ MJ}$.

The temperature of the storage seems to stabilize after some 4 – 5 h, as an example Figure 5.1.a and Figure 5.1.b show the temperatures. This means that the heat loss at this temperature, 145 K, is 600 W, and the temperature difference to the environment $\Delta T_{SE2} = 145 - 35 = 110 \text{ K}$. Correspondingly, the mean temperature difference to the environment during charging is some $90 - 25 = \Delta T_{SE1} = 65 \text{ K}$. Since heat loss, both due to convection and radiation increase more than linear with temperature, it is reasonable to assume that the difference between ΔQ_{In2} and ΔQ_A is due to heat loss.

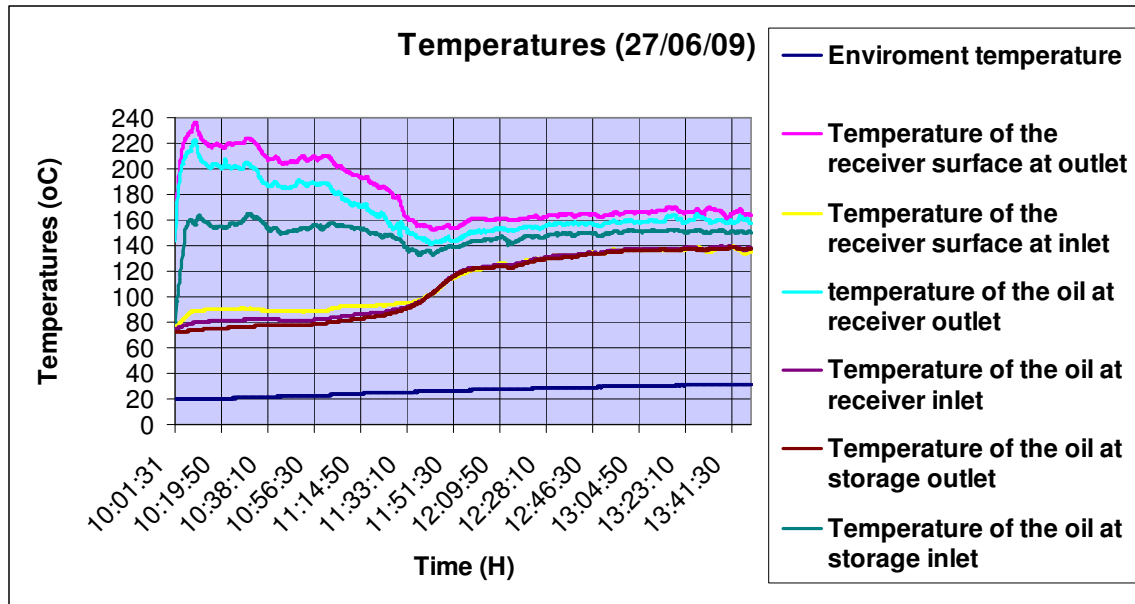


Figure 5.2.a: Results of temperatures measurements, on 27th June, 2009.

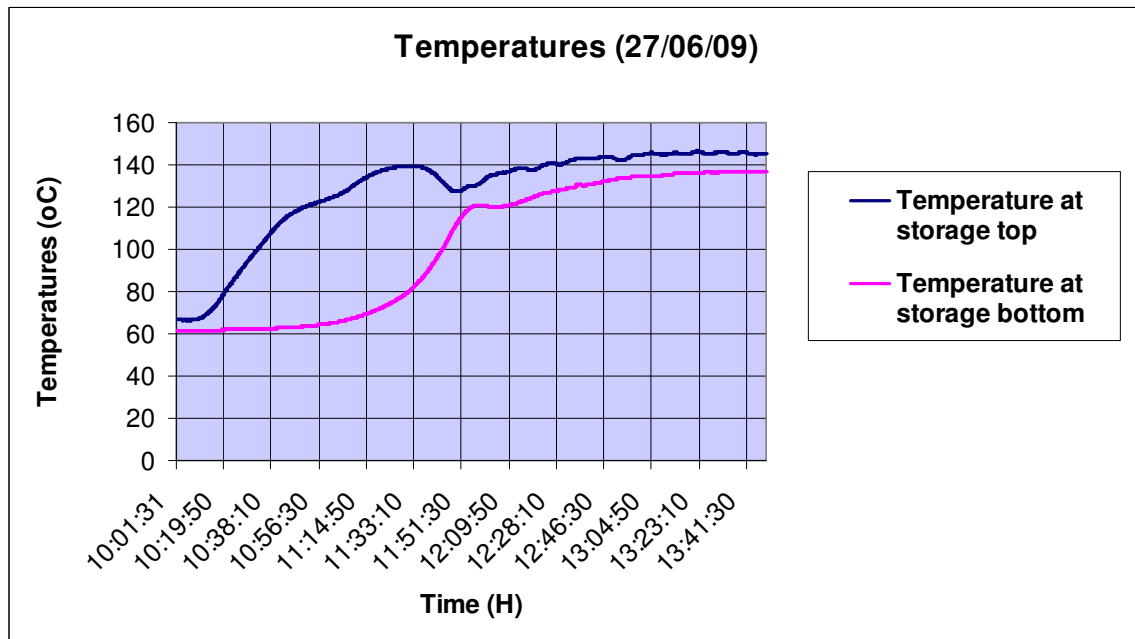


Figure 5.2.b: Results of temperatures measurements inside storage, on 27th June, 2009.

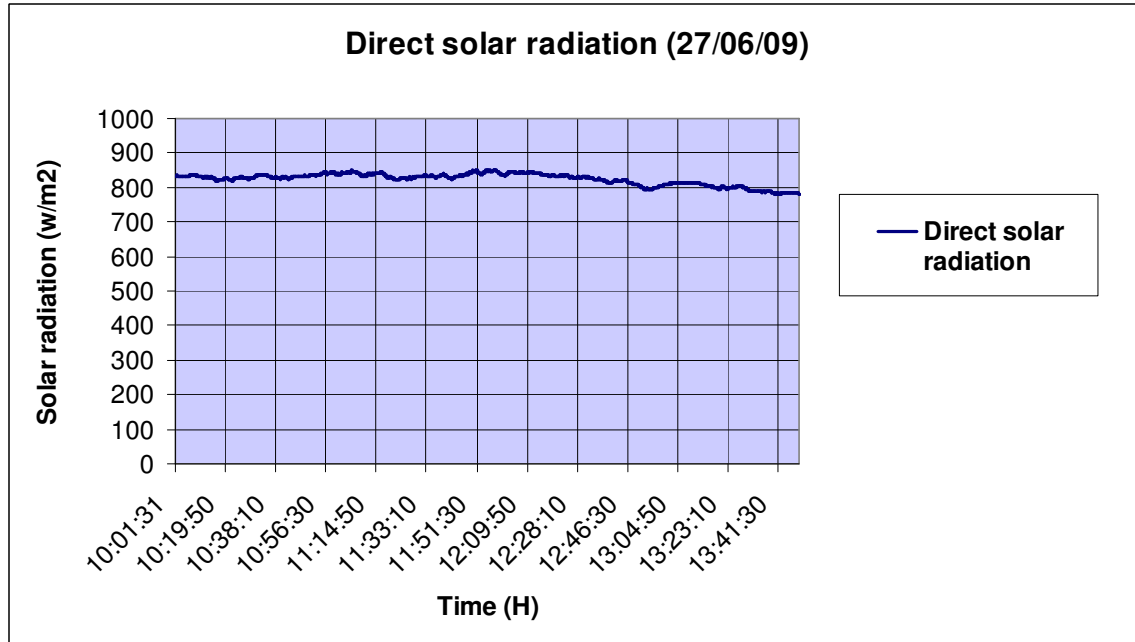


Figure 5.2.c: Results of direct solar radiations measurements, on 27th June, 2009.

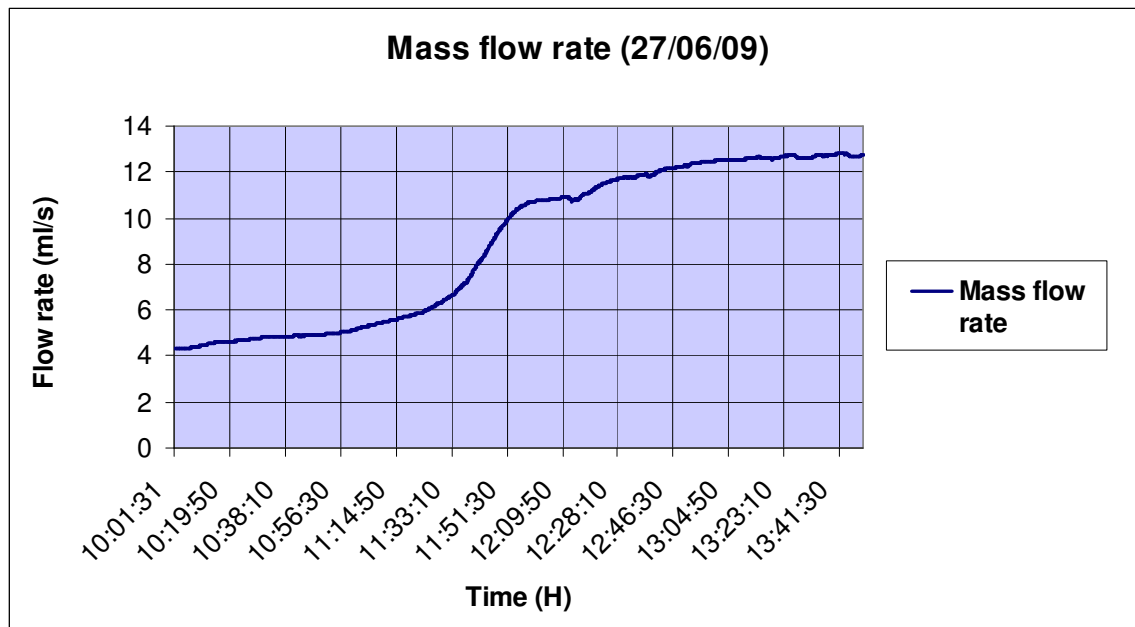


Figure 5.2.d: Results of mass flow rate measurements, on 27th June, 2009.

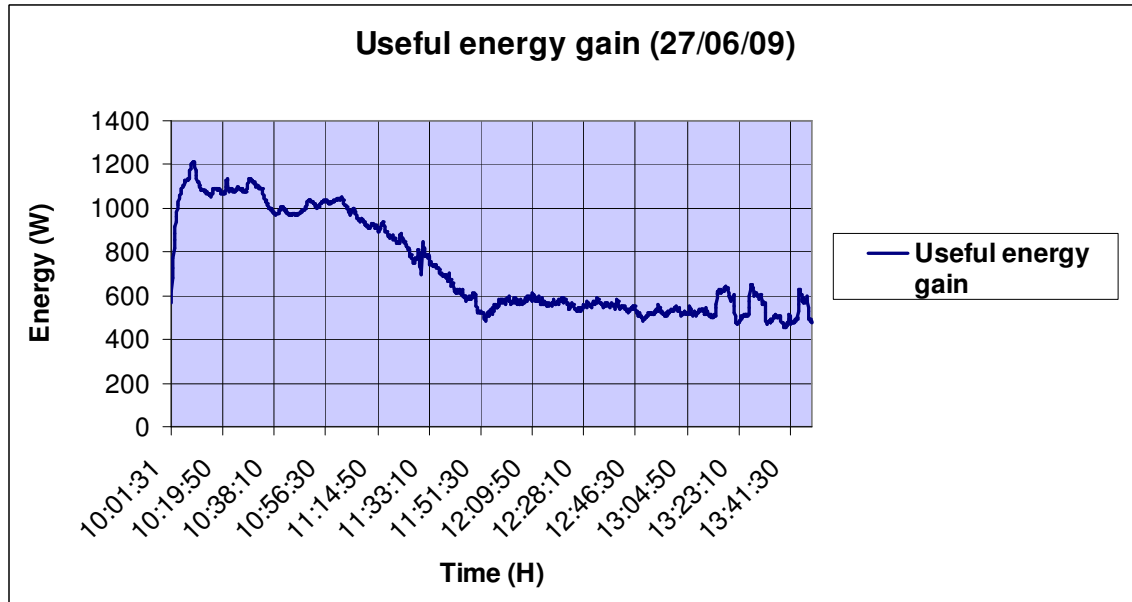


Figure 5.2.e: Useful energy gain on 27th June, 2009.

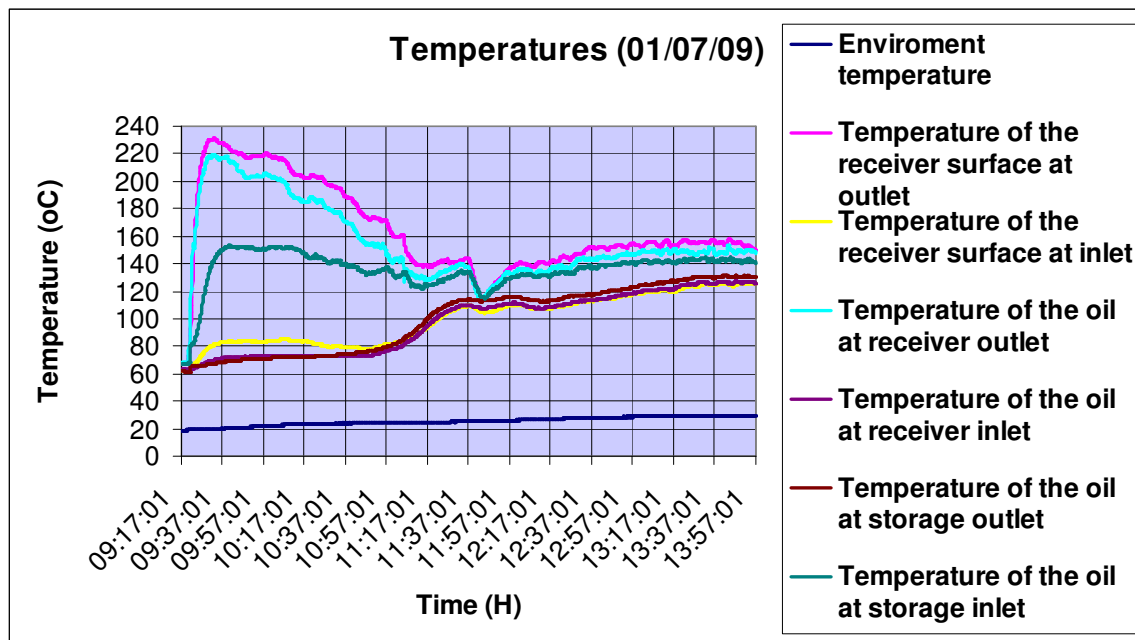


Figure 5.3.a: Results of temperatures measurements, on 01st July, 2009.

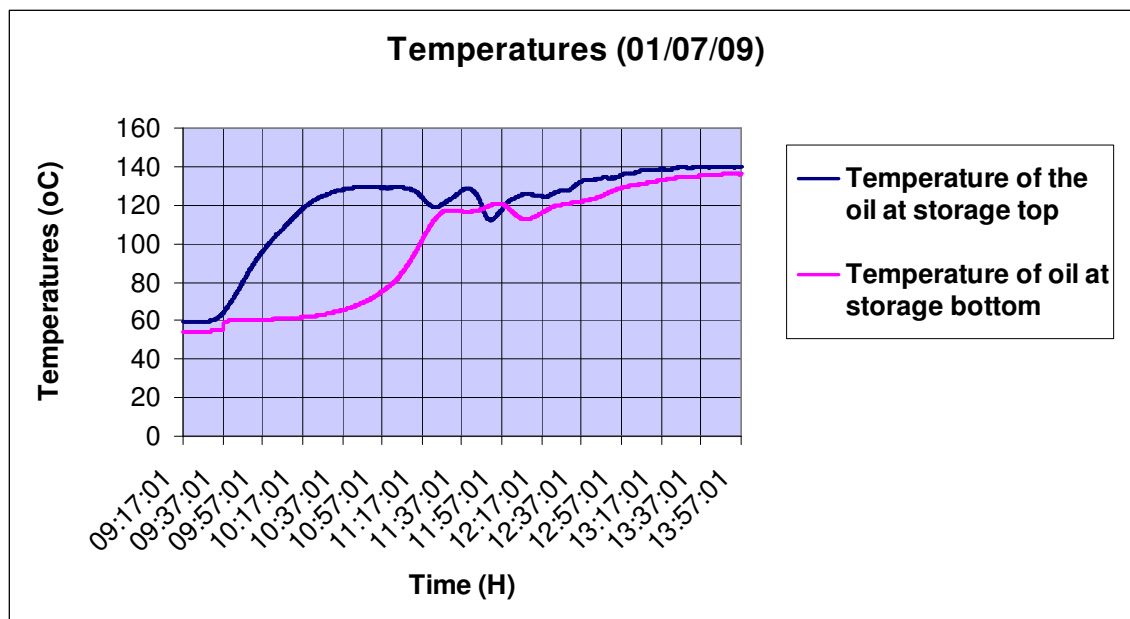


Figure 5.3.b: Results of temperatures measurements inside storage, on 01st July, 2009.

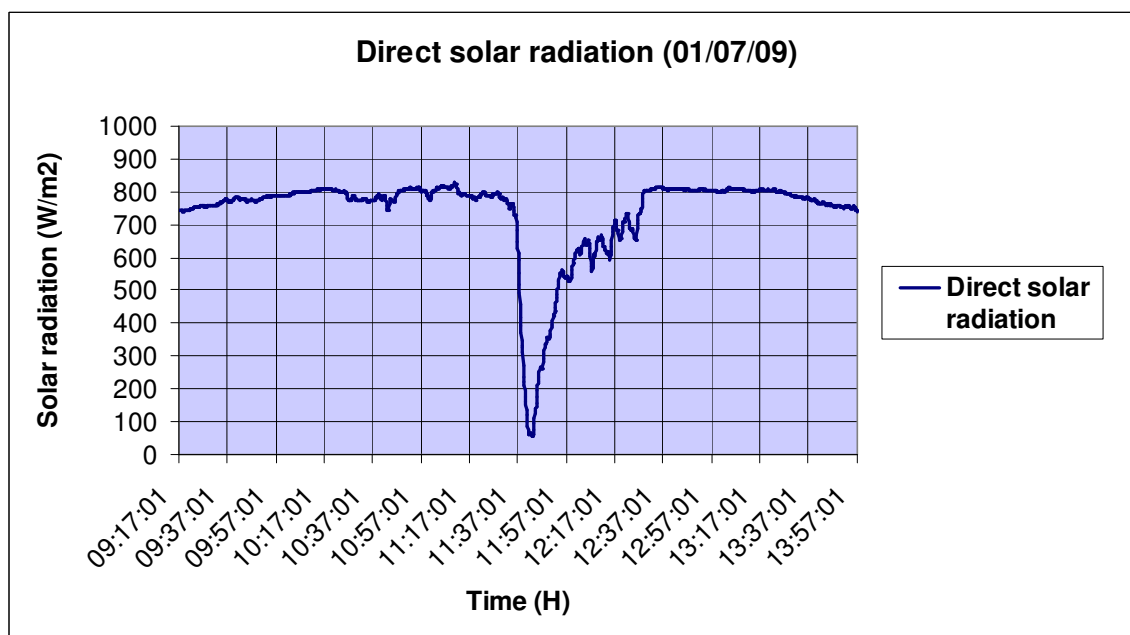


Figure 5.3.c: Results of direct solar radiations measurements, on 01st July, 2009.

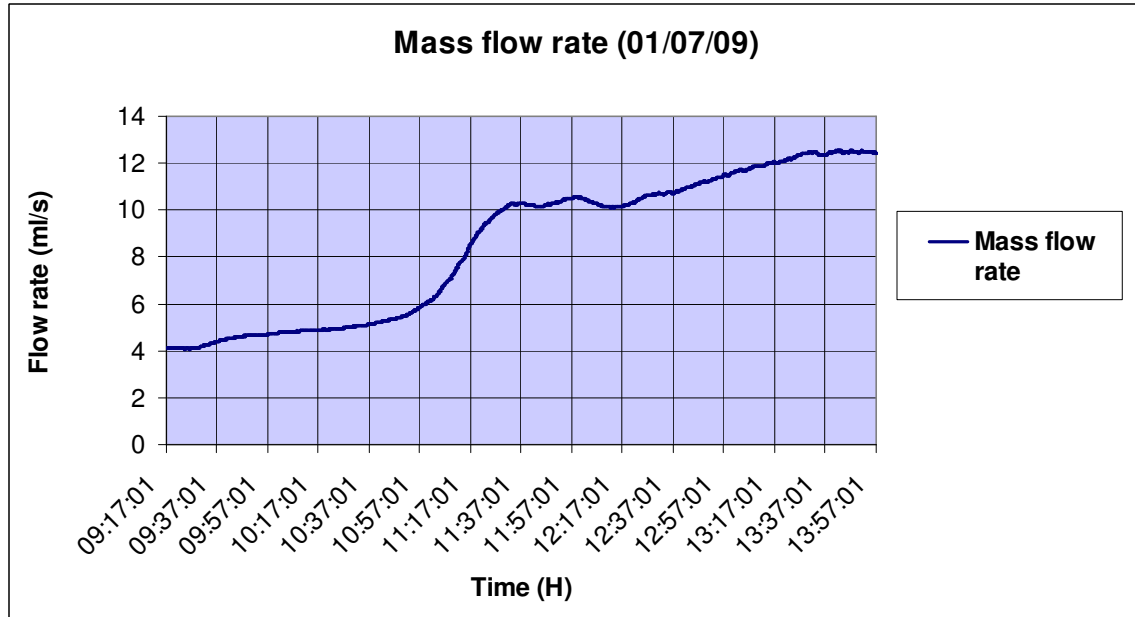


Figure 5.3.d: Results of mass flow rate measurements, on 01st July, 2009.

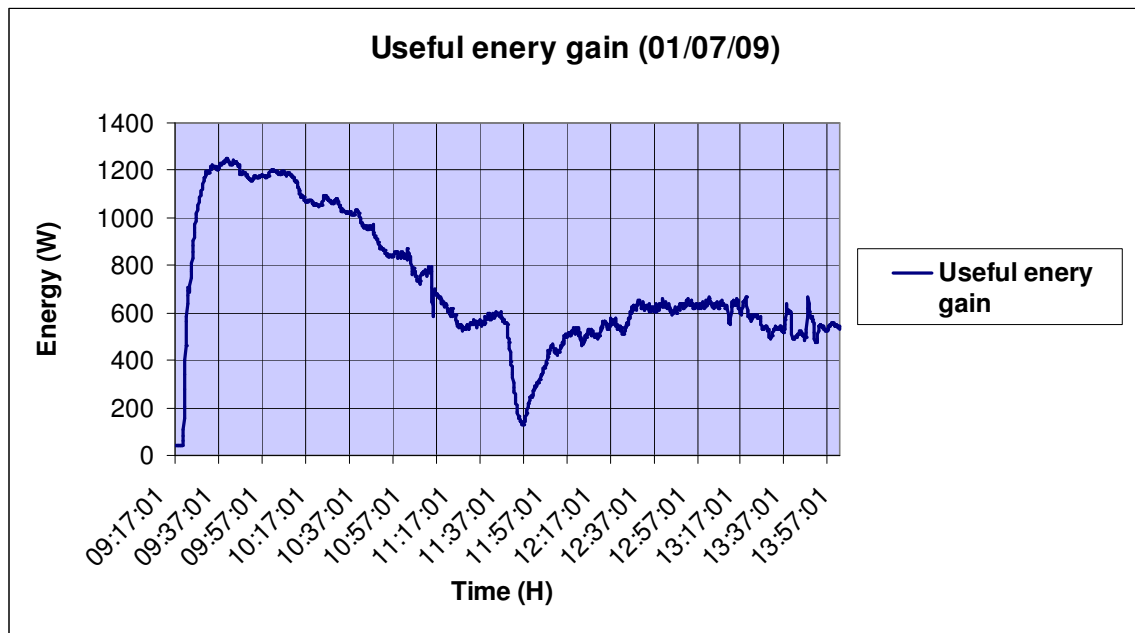


Figure 5.3.e: Useful energy gain on 01st July, 2009.

The oil flow rate decreases when the solar radiation intensity decreases since the temperatures decrease as indicated in Figures 5.3.d, 5.3.c and 5.3.a respectively. In this

day (1st July 2009) we had a period of cloudy coverage and the solar radiation achieved the lowest intensity of 55 W/m^2 , at 11:42:51 hours within time interval along with the temperature was measured. Obviously, this cloudy coverage affected negatively the receiver temperature, the oil temperature at outlet of the receiver and the oil temperature at the inlet storage. Consequently the temperature inside storage also decreased and all other parameters measured were affected. This shows the dependence between the measured parameters.

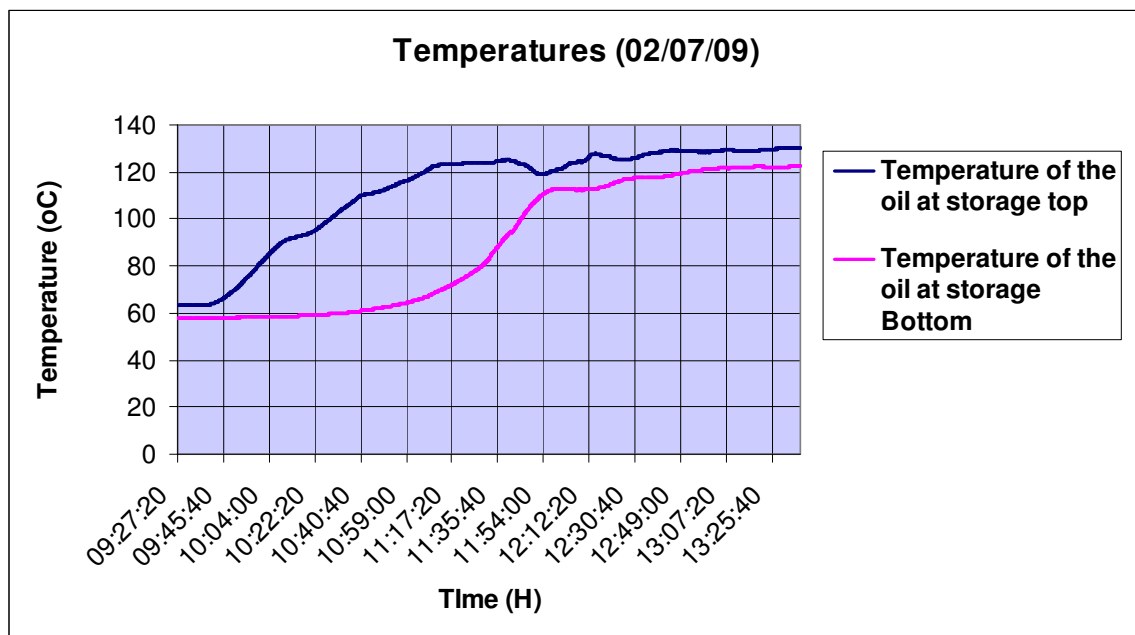


Figure 5.4.a: Results of temperatures measurements inside storage, on 02nd July, 2009.

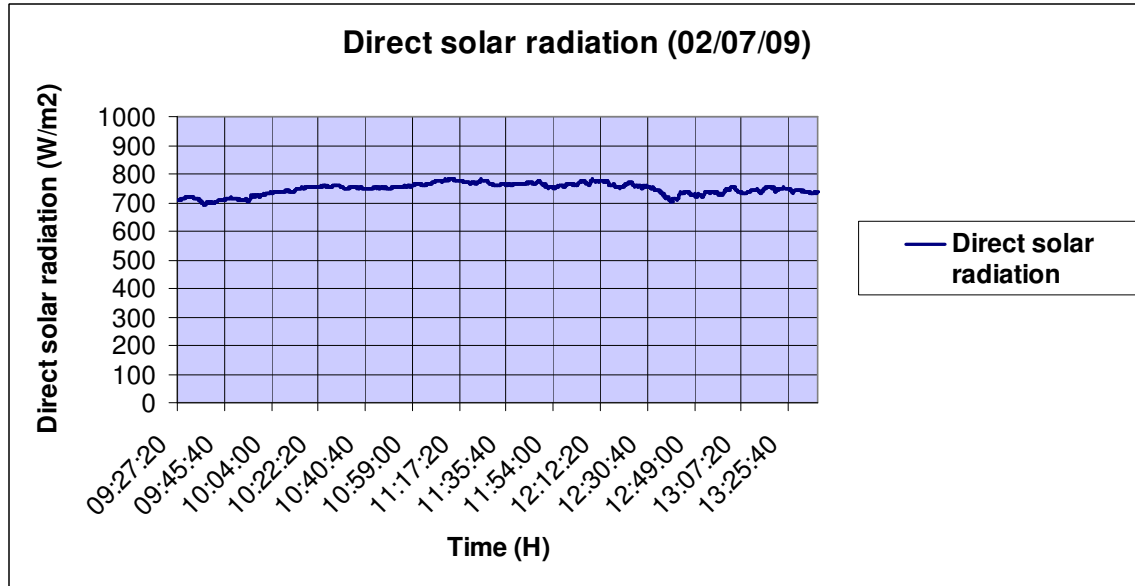


Figure 5.4.b: Results of direct solar radiations measurements, on 02nd July, 2009.

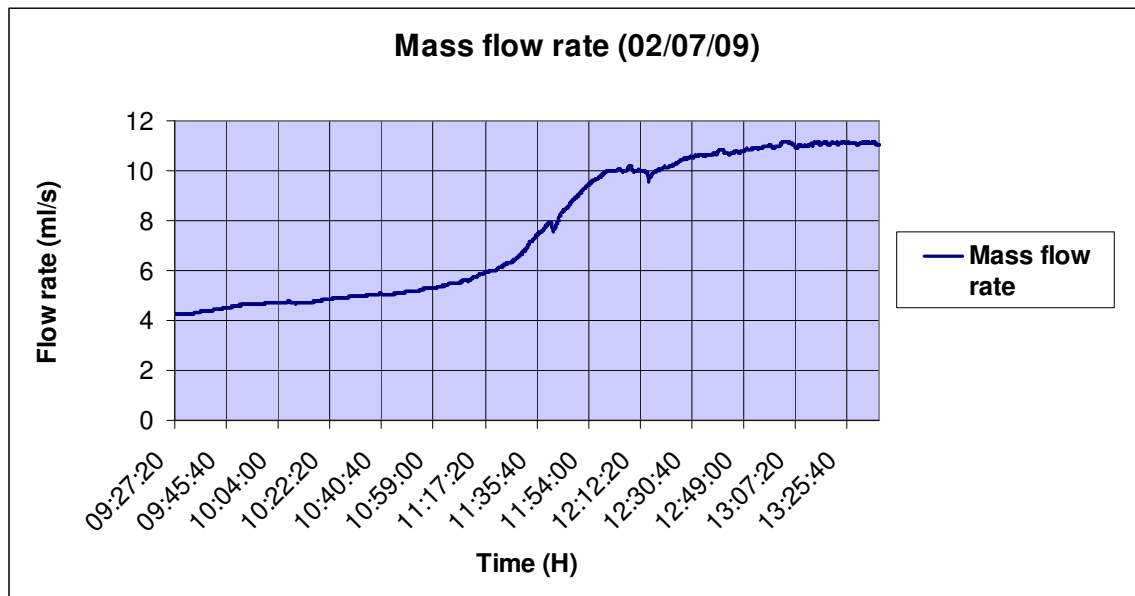


Figure 5.4.c: Results of mass flow rate measurements, on 02nd July, 2009.

Comparing Figures (5.1.a, 5.2.a and 5.3.a) indicates that they display similar behavior. In the temperature diagrams the oil temperature and the temperature of the receiver surface at the outlet are high during approximately one and half to two hours counting from the beginning of pumping process. This is due to the low flow rate of the oil.

The temperature behavior in figures 5.1.a and 5.2.b can also be seen in figures 5.2.a and 5.2.b from 10:01:31 hours to 10:33:10 hours, in figures 5.3.a and 5.3.b from 09:17:01 hours to 10:57:01 hours and in figures 5.4.a from 09:27:20 hours to 11:17:20 hours. With the increase of the oil flow rate the receiver temperature is reduced. This variation of temperature is also seen for the oil at receiver outlet, storage inlet and storage top for the same time interval. The temperatures reduce also due to the lack of insulation in the storage and transfer pipes.

Sometimes the temperature of the oil is higher than the temperature of the receiver surface because the thermocouple connected to read the receiver surface temperature is from the backside of the receiver, and obviously the temperature at the side of solar exposure is much higher. This is verified in the first minutes of the temperature readings. In all cases, the apparent energy gain is higher in the morning and lower in the afternoon when the input oil is heating up. This is probably due to malfunction of the pump.

5.1. Efficiency of the system

The environmental temperature and weather, particularly the wind, greatly affect the performance of the system. Part of heat is lost in the pipes that connect the receiver to the storage (a pair of about 4 meters of length each). These pipes are too long, which increase the losses. As seen in figure 5.1.f, the losses to the environment are high. Temperatures over 150°C inside storage can be achieved with better weather conditions. The oil flow rate is laminar during all pumping process since the Reynolds number is lower than 4000. As an example, for the high oil flow rate the Reynolds number was about 1700. A better pump which can produce a turbulent oil flow rate is necessary. Despite high losses of heat, the system has shown that it has capability to produce high temperatures. Figure 5.5 shows the graphic of the efficiency of the system.

Since the temperature used to calculate the efficiency is the temperature at inlet and outlet of the receiver, heat loss is the smaller part of the problem. Imperfect focusing is the major problem in the system.

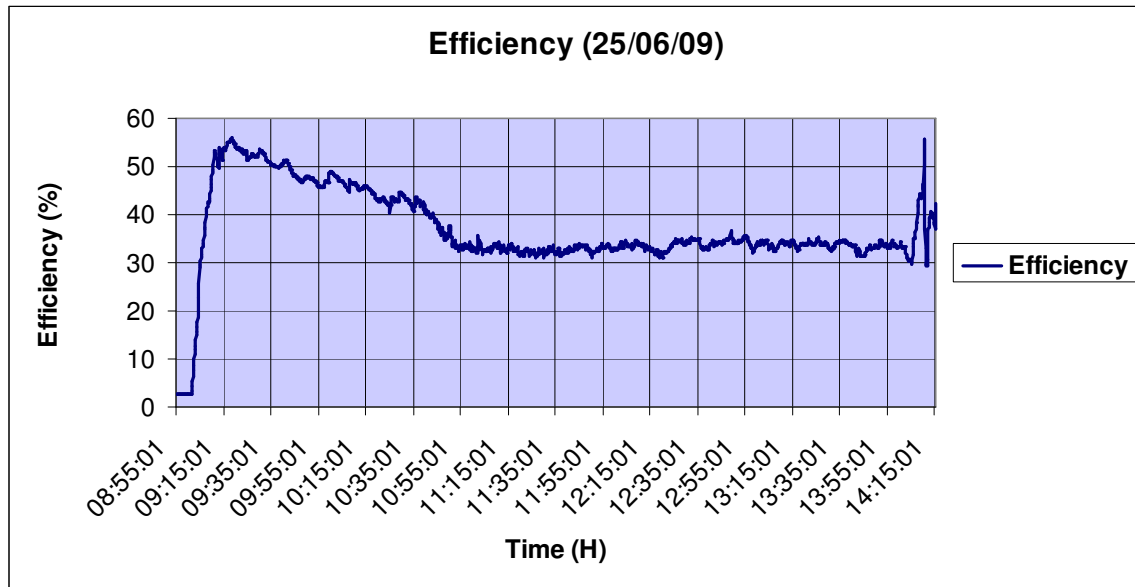


Figure 5.5: Efficiency of the system on 25th June 2009.

The efficiency of the system is about 35% considering the values of the heated oil, in figure 5.5, from 10:55 hours backward there is the mentioned problem with the oil back leakage at the pump.

Chapter 6

Conclusions and Future Work

A solar radiation concentrating collector was designed, constructed and evaluated. It was concluded that, the solar radiation concentrating system is capable of producing enough heat for food preparation and water pasteurization which is the main objective. Stored energy achieved temperatures of about 150°C. The maximum daily average of efficiency was about 35%. This efficiency can be improved by better insulation of the receiver (storage and transfer pipes were not insulated in this test) and sharper focus (misaligned tiles caused part of solar radiation to not strike the receiver).

The life time of the concentrator made by grouped tiles should be studied separately, since the spot of solar radiation reflected is becoming large with time. This can be due to errors during the construction of the concentrator or the concentrator is being deformed due to weather conditions.

The Calflo heat transfer fluid can be used as heat transfer fluid. The disadvantage is that this oil has poor heat conductivity and a bad smell when heated. For a solar oven the storage must be relatively far from kitchen and all oil leakage avoided.

For possible future work a full dish, instead of half is a good option. Half dish reduces the geometric concentration ratio and increase thermal losses, since considering the other half with same slop errors as the present half dish to complete a full dish, the receiver dimensions should have been the same. Selective absorbers are also necessary to improve the receiver heat loss by IR radiation. A full dish can use the same receiver as half dish, but will double the heat input. Loss from the receiver and transfer piping will be similar, but large storage will increase heat loss somewhat.

All temperature sensors in the storage should be read in order to estimate a mean temperature in the storage during charging. Also time series of temperature during cooling should be established. From these curves, heat loss and gain may be studied as a function of temperature, and a better understanding of the system properties will be possible to achieve. Before that, the system should be thoroughly revised, insulated and improved.

References

1. Arenas J., '*Design, development and testing of a portable parabolic solar kitchen*', Renewable Energy 32, 257–266, (2007).
2. Buddhi D.; Sahoo L., '*Solar cooker with latent heat storage: design and experimental testing*', Elsevier, Volume 38, Number 4, pp. 245-245(1) (1997).
3. Bushnell DL., '*Performance studies of solar energy storing heat exchanger. Solar Energy*', 41(6): 503–12, (1988)
4. Campbell and Green, '*The limiting efficiency of silicon solar cells under concentrated sunlight*', volume 13, (1987).
5. Cuamba B., Chenene M., Mahumane G., Quissico D., Lovseth J. and O'keefe P., '*A solar energy resources assessment in Mozambique*' Journal of Energy in Southern Africa, volume 17, No. 4, (2006).
6. Cuamba B., Chenene M., Domingos A., Lovseth J. and Nydal O., "*Design and Construction of a Sun tracker for Use in Low Cost Small Scale Multipurpose Thermal Solar Energy Concentrating Systems*", World Renewable Energy Congress: 1880, (2008).
7. Domanski R, El-Sebaï A. and Jaworski M., '*Cooking during off-sunshine hours using PCMs as storage media. Energy*', 20(7):607–16 (1995)
8. Duffie J. and Beckman W., '*Solar Engineering of Thermal Processes*', 2nd Edition, (1991).
9. Franco J., Saravia L, Javi V., Caso R. and Fernandez C., '*Pasteurization of goat milk using a low cost solar concentrator*', Solar Energy 82, 1088–1094, (2008).

10. Hewlett Packard, HP 34970A Data Acquisition/Switch Unit User's Guide, Hewlett Packard Company, Colorado (1997).
11. Imadojemu H., '*Concentrating Parabolic Collectors: A Patent Survey*', volume 36, No. 4, 225-237, (1995).
12. Johnston G., Lovegrove K. and Luzzi A., 'Optical performance of spherical reflecting elements for use with paraboloidal dish concentrators', *Solar Energy* 74, 133–140, (2003).
13. Kaushika N. and Reddy K., '*Performance of a low cost solar paraboloidal dish steam generating system*', *Energy Conversion & Management* 41, 713-726, (2000).
14. Kaneff S., '*Commercially Viable Solar Thermal Power Systems in the Range 50 kWe to 100 MWe*', (1995).
15. Lovseth J., '*Personal notes*', (2008).
16. Lovseth J⁽¹⁾., '*Heat Transfer Methods from Absorber to Storage*', Annual Small Scale Concentrating Solar Energy Systems Workshop, Makerere University, Kampala - Uganda, 18 - 19, September, (2008).
17. MacDonald G. and Sertorio L., '*Global climate and ecosystem change*', Volume 240, (1990).
18. Mawire A. '*A data acquisition and control system for a solar thermal energy storage (TES) and cooking system,*' A thesis submitted in fulfillment of the requirements for the degree of Master of Science in Applied Physics in the Faculty of Science and Agriculture at the University of KwaZulu-Natal, (2005).

19. Mills D., '*Solar Thermal Electricity*', Solar Energy, State of the Art, ISES position papers – Jeffrey Gordon (Editor), pg 577 (2001).
20. Mills D., '*Advances in Solar Thermal electricity technology*', Solar Energy 76, 19-31 (2004).
21. Morrison G., '*Solar Collectors*', Solar Energy, State of the Art, ISES position papers – Jeffrey Gordon (Editor), pg 145 (2001).
22. National Directory of energy (Mozambique), (2006)
23. Nijegorodov, N., Devan, K., Simao, H., Mabbs, R., '*Comprehensive study of solar conditions in Mozambique: the effect of trade winds on solar components*' Renewable Energy 28, 1965–1983 (2003).
24. Nordlander S., '*Maximum Concentration for Ideal Asymmetrical Radiation concentrators*', Solar Energy 79, 566 (2005).
25. Norton B., '*Solar Process Heat: Distillation, Drying, Agricultural and Industrial Uses*', Solar Energy, State of the Art, ISES position papers – Jeffrey Gordon (Editor), pg 497 (2001).
26. "Oil hits \$100 barrel". BBC News.
27. Ramadan M, Aboul-Enein S and El-Sebaei A., '*A model of an improved low cost indoor. Solar Wind Technol*', 5(4):387–93, (1988).
28. Scheffler, Papers 20, SCI Conference, 2006/21
29. Stine B. and Geyer M., '*Power From The Sun*,' (2001).

30. Twidell J. and Weir T., '*Renewable Energy Resources*', 2nd Edition, New York, (2006).
31. Timinger A., Spirkel W., Kribus A. and Ries H., '*Optimized secondary concentrators for a partitioned central receiver system*,' Solar Energy 69, 153-162, (2000)
32. Toonen H., '*Adapting to an innovation: Solar cooking in the urban households of Ouagadougou (Burkina Faso)*', Physics and Chemistry of the Earth 34, 65–71, (2009).
33. van den Heetkamp R., 'Personal draft', (2007).
34. Winston R., '*Solar Concentrators*', Solar Energy, State of the Art, ISES position papers – Jeffrey Gordon (Editor), pg 393 (2001).
35. Website 1: <http://www.ivt.ntnu.no/ept/NUFUSolar/>
36. Website 2 (<http://calflo/tech-sheets.htm>)
37. Website 3 (www.cmdl.com)
38. Website 4 (www.omega.com)
39. (Some Photographs): Ole Jorgen Nydal, Professor Energy and Process Engineering Norwegian University of Science and Technology, 7491 NTNU, Trondheim, Norway.